Spatiotemporal Urban Flood Expansion and Propagation by Percentage of Node in Flood Assessment (PNFA)

Short title: Spatiotemporal analysis of flood caused by combined sewer system in Viet Nam

Ha Do Minh[1,2,4*], Gerald Augusto Corzo Perez[1,2], Wilmer Barreto[3], Chris Zevenbergen[1,2]

[1] IHE Delft Institute for Water Education, Westvest 7, 2611 AX Delft, Netherlands.

[2] Faculty of Civil Engineering and Geosciences, Delft University of Technology (TU Delft), Stevinweg 1, 2628 CN Delft, The Netherlands.

[3] Department of Civil Engineering and Geology, Catholic University of Temuco, Manuel Montt 056, La Araucanía, Chile.

[4] Faculty of Infrastructure and Environment Engineering, Ha Noi Architectural University, Km10, Nguyen Trai, 11400 Thanh Xuan, Ha Noi, Viet Nam.

* Corresponding author. Email: h.do@un-ihe.org.

Peer review status:

This is a non-peer-reviewed preprint submitted to EarthArXiv.

This manuscript is now under review of Hydrology Research Journal.

ABSTRACT

Urban pluvial flooding is a complex process shaped by rainfall intensity, drainage system capacity, and urban infrastructure. While previous studies have mapped flood extents, the spatiotemporal evolution of drainage saturation and overflow propagation remain insufficiently explored. This study introduces the Percentage of Node in Flood Assessment (PNFA), integrating the Flood Expansion Rate (FER) to measure flood spread within drainage networks. Using the EPA Storm Water Management Model (SWMM), three historical storms (2008, 2019, 2020) and seven returned period scenarios were simulated in Do Lo, Hanoi, Vietnam.

Results reveal that despite variations in rainfall intensity, spatiotemporal flood patterns remain stable, suggesting predictable flood propagation pathways. FER values range from 0.17 (slow) to 0.902 (rapid), indicating that system response is highly sensitive to storm intensity. Key flood-prone areas consistently experience early drainage saturation, pinpointing critical intervention points. Flood propagation speed and saturation timing are crucial for early warning systems and emergency response strategies.

This study enhances urban flood risk assessment by incorporating spatiotemporal flood hazard mapping, which considers the sequence and timing of flood events. These insights are crucial for flood mitigation, urban planning, and drainage system resilience, highlighting the importance of time-sensitive flood risk models amid rising extreme weather events.

KEYWORDS

spatiotemporal flood, flood hazard map, urban flood, urban drainage system, pluvial flood, PNFA.

GRAPHIC ABSTRACT

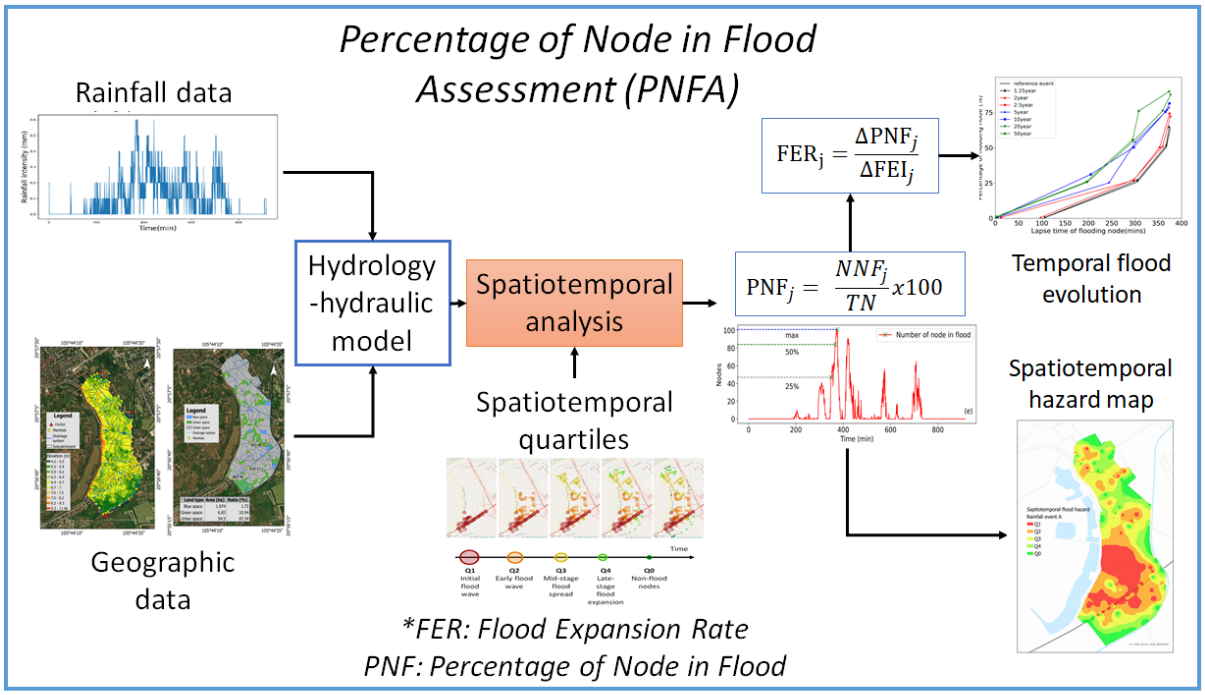

HIGHLIGHTS

- Percentage of Node in Flood Assessment (PNFA) includes temporal and spatiotemporal analysis.
- 5 spatiotemporal flood quartiles represent flood evolution during the flooding time.
- Flood Expansion Rate (FER) is a measurement assessing the spatiotemporal flood agility.
- Flood evolution diagram shows the actual flood expansion agility spatiotemporally.
- Spatiotemporal flood hazard map gives new insight to flood management.

INTRODUCTION

Pluvial flood generally receives less attention from both citizens and researchers because of its small scale and low-cost damages. Pluvial flood is characterized as scattered in distribution, sudden onset, spatial and temporal unpredictability, and short duration. A holistic understanding of this flood type is required but still remains as a challenge for scientists (Schanze, 2018). At first glance, damages caused by pluvial flood events appear to be less severe comparing to fluvial flood events. However, pluvial floods annually occur more frequently on an annual basis (Acosta-Coll *et al.*, 2018). Furthermore, under the influence of climate change, the number of pluvial floods, which are triggered by intensive rainfall, is increasing (Kundzewicz and Pińskwar, 2022). Despite causing lower-cost damages per event, the high frequency of pluvial floods results in annual damage comparable to that of occasional fluvial flood, especially in megacities (Tanaka, Kiyohara and Tachikawa, 2020).

In addition, urban floods also threaten the public health by its water quality. Combined drainage systems are employed in most cities worldwide due to their cost-effectiveness. However, these systems are also a source of contamination during flooding. When the drainage systems become overloaded, a mixture of rainwater and domestic wastewater overflows through manholes, resulting in localized flooding around the affected areas. This over-spilled mixture potentially increases the risk to public health when the dwellers are exposed to it (Nguyen *et al.*, 2017; Huynh *et al.*, 2019; Olsson, 2019; Beg *et al.*, 2020). As a result, 60% of the global population living in cities faces health risks from flooding. Furthermore, as rapid urbanization continues, flood-prone areas expand, placing an increasing number of citizens in danger (Güneralp, Güneralp and Liu, 2015). Hence, the contribution of domestic wastewater to urban pluvial flood could not be overlooked. A profound understanding of pluvial floods in the context of urban areas is necessary to alleviate the pluvial flood damage and mitigate the flood risk.

In spite of extensive research, the intricate nature of the drainage system network still poses challenges for scientists to understand the urban pluvial floods spatially and temporally (Francipane *et al.*, 2021). The spatial distribution of rainfall, even on a small scale, plays a crucial role in the evolution of floods due to the complex precipitation patterns (Prokić, Savić and Pavić, 2019). Moreover, the pathway and intensity of urban floods are subjected to change, influenced by the heterogeneous characteristics of drainage systems and the dynamic distribution of storms (Leandro, Schumann and Pfister, 2016). It is essential to consider the trade-offs between drainage system capacity and spatiotemporal rainfall intensity to understand the dynamics of flood hazards in urban environments in term of the hydrological and hydraulic aspects.

This study aims to introduce a novel method for analysing urban pluvial flooding from a spatiotemporal perspective. The dynamics of flood events were examined, with a focus on their spatial and temporal distribution. The methodology was applied to an urban area, Do Lo, located in Yen Nghia Precinct, Ha Dong District, Hanoi, Vietnam, as a representative case study. The objectives are to: (i) examine the spatiotemporal heterogeneity of urban flood hazards under extreme rainfall events and (ii) identify key factors influencing flood dynamics in specific regions. The study aims to provide insights into flood location and intensity, leading to a spatiotemporal flood hazard map that classifies hazards by both space and time. Additionally, it proposes a simple method for comparing flood extremes. Integrating time into flood risk assessment can enhance preparedness, particularly in optimizing resource allocation for evacuation planning.

This research focused on the hydrological aspect of flood hazards including modelling, analysing flood speeds, and generating spatiotemporal hazard maps. The paper is structured into 7 sections: (1) Introduction, providing an overview of spatiotemporal flood analysis research; (2) Background, presenting the research gaps in flood assessment; (3) Study Area,

detailing the hydrological characteristics of the case study; (3) Materials and Methods outlining the Data sources, Research method and PNFA method; (4) Results, presenting modelling results and PNFA analytical findings; (5) Discussion; and (6) Conclusion.

BACKGROUND

Conceptual physically based models are widely employed to simulate and characterize floods in urban areas (Getirana *et al.*, 2023; Lameche *et al.*, 2023; Hauser *et al.*, 2024; Sañudo *et al.*, 2024). These models, which specially focus on flood hazards, involve two key concepts: firstly, the determination of the saturation point in specific locations within the network's manholes; and secondly, the representation of the flow dynamics of water volume and its connection to the existing runoff on the streets. The integration of 1D and 2D hydrodynamic models allows a comprehensive understanding of urban floods (Leandro *et al.*, 2009; Seyoum *et al.*, 2012). However, the focus of flood management in urban systems primarily revolves around drainage systems, as they are the key infrastructure objects designed and maintained by humans. Many studies utilized the EPA Storm Water Management Model (SWMM) to estimate the location and intensity of inundation by identifying saturation points in manholes (Piadeh, Behzadian and Alani, 2022). The captured flood hydrodynamics in those previous studies could provide insights into the capacity and behaviours of the overall network. Although it offers direct information on flood event locations and timing, these complex networks require additional analysis steps to fully understand the flood evolution and flood patterns.

Therefore, understanding the drainage saturation and flood starting point is the beginning of an analysis, as demonstrated in several studies (Mishra, Sethi and Siddique, 2020; Afsari *et al.*, 2022; Levin and Phinn, 2022; Zhou *et al.*, 2022; Wijaya *et al.*, 2023). This information allows us to understand the areas at flood risk and also how to effectively map the flood risk in a city. However, the concept of flood risk has often been restricted to static representations. Many

studies often overlook the dynamic nature of floods in terms of hazard analysis (Arrighi, Oumeraci and Castelli, 2017; Dong *et al.*, 2022; Li *et al.*, 2023). The sequential pattern of saturation across various urban areas and the involved water volume can be vary significantly. This information is crucial for assessing the danger level posed to citizens. Recognizing the hazard concept, which involves analysing the water force capable of carrying individuals or vehicles, is pivotal. This perspective highlights the potential devastating impact of even a simple flood due to its kinetic energy (Zhu *et al.*, 2023).

Furthermore, a sufficient time for reaction to flood will reduce damage costs. In case of flash flood, where the flood caused in rapid onset under the intense rainfall, speedy responses showed the serious practical consequences (Archer and Fowler, 2018). Early flood warning system has been being a useful system for flood preparedness in the transition area from structural to non-structural flood measurement. Real-time forecasting helps decision makers foreseen the disaster situations and be proactive in making emergency response plans (Henonin *et al.*, 2013; Mahiddin, Umar and Rajan, 2023). Time is crucial element in effective flood warning messages (Kuller, Schoenholzer and Lienert, 2021; Fernández-Nóvoa, González-Cao and García-Feal, 2024). Consequently, considering not only the spatial distribution but also the temporal distribution in flood risk assessment are necessary to fulfil the flood risk information for flood management tools (e.g. flood hazard maps) (Wang *et al.*, 2022; Corzo Perez *et al.*, 2024). Therefore, it is crucial to study the dynamics of flood initiation, the time it takes for floods to reach critical points, and the overall spatiotemporal saturation patterns in the drainage network.

Nevertheless, research on flood dynamics is rare and often lack integration of all aforementioned aspects. It required comprehensive flood risk frameworks. Recently, time scale was considered in flood analysis. The term “spatiotemporal” is commonly used in long-term and large-scale flood analysis, where the temporal scale typically refers to a yearly timeframe.

147 For example, flood events during period 1985-2019 were classified globally based on the flood
148 affected area (Liu, Shi and Fang, 2022). Under continental view, flood extent trends in Europe
149 were explored in last 70 years (Fang *et al.*, 2024). In national scale, the long-term
150 spatiotemporal pattern of flood exposure in US through 2 decades from 2001 to 2019 was
151 investigated (Abedin *et al.*, 2024). The effect of changing land use and land cover to flood
152 behaviour were assessed by flood exposure throughout three decades (1992-2022) in Bangkok
153 Metropolitan Region (Darnkachatarn and Kajitani, 2024).
154 Recently, some researchers have examined spatiotemporal patterns at the event scale rather
155 than the yearly timeframe. The spatiotemporal dynamics of rainfall distribution also affected
156 the flood response in surface and subsurface (e.g. drainage systems) (Zhou *et al.*, 2021). The
157 spatial and temporal variations in rainfall distribution influenced the location of pressurized
158 flow, leading to geyser-like streams on the street (Vasconcelos *et al.*, 2024). Spatiotemporal
159 flood hazard was initially analysed using a combination of traditional modeling and machine
160 learning. Although flood evolution was presented in hourly flooding time steps, the temporal
161 flood distribution was presented in a sequence of spatial flood maps (Lee *et al.*, 2020). In the
162 built environment, a time-depending model was introduced for flood risk assessment
163 incorporating user characteristics. Flood risk was assessed and calculated for each categorized
164 group based on individuals' vertical position within the building and their home presence
165 duration. Flood evacuation routes, as a result, were designed based on spatiotemporal flood
166 risk analysis (Bernardini *et al.*, 2024). As the underground spaces of buildings are vulnerable
167 to flood, time is an important factor affecting flood risk and escape routes beside flood
168 prevention measurement (Shin *et al.*, 2021).
169 Meanwhile, data driven models – a flood forecast approach using machine learning and deep
170 learning techniques also considered the time scale. Flourished in data era, data-driven models
171 have become more robust to predict the flood. Machine learning techniques are used to leverage

flood forecast. In order to predict coastal urban pluvial flooding, a machine learning model was used to generate the missing drainage data (i.e. point of water logging depth) to enhance the calibration process for traditional models (Qin *et al.*, 2024). Artificial neural networks (ANN) were introduced to predict spatial flood maps. In addition to predicting water depth, temporal flood evolution was considered separately as a sequence of spatial flood maps (Berkhahn and Neuweiler, 2024; Zhou *et al.*, 2025). Shallow-water-equation-inspired graph neural network (e.g. Delft3D-FM) was introduced to predict dike breach flooding. This model successfully predicted the spatial flood distribution over time. However, that research focused on flood forecasting capabilities but has not yet developed a flood risk assessment – which is needed for end-users (Bentivoglio *et al.*, 2023). Several other studies have combined machine learning and physical-based model results to improve flood prediction. For example, a graph neural network was combined with MIKE+ model results to predict pluvial urban flooding (Burrichter *et al.*, 2023). A convolution neural network combined with HEC-RAS model results were used to predict the spatiotemporal fluvial flood in an urban area (Schmid and Leandro, 2024). Urban flood inundation maps were generated using a fused model that combined Principal Component Analysis (PCA), Self-Organizing Map (SOM) and Non-linear Autoregressive with Exogenous Input(NARX) (Chang, Liou and Chang, 2022). Recent data driven models have mainly focused on representing flood maps. While time scales were considered in sequences of spatial flood maps, however they have not been effectively utilized in developing flood hazard maps. Therefore, the integration of the temporal scale into flood assessment, along with the development of appropriate methodologies, is becoming increasingly essential.

STUDY AREA

The study area, Do Lo, is located in the southwest of Yen Nghia Ward, Ha Dong District, the fringe of Ha Noi City, Viet Nam (Figure 1a). This urban area was transformed from two old

196 villages, as decided by The Government(Vietnam Government, 2006, 2008). There were
197 10,373 residents living in this 61.5 ha area in 2019 (Yen Nghia Comune People's comittee,
198 2019). Do Lo, Yen Nghia is a dense urbanized area with a population density of approximately
199 16,900 persons/km^2.
200 The case study has a tropical and monsoonal climate with 4 distinct seasons (i.e. spring,
201 summer, autumn, and winter). Average temperature is +23°C, ranging from+5ºC to +38°C.
202 Rainy season (from May to October) coincides with Asian monsoon (Ho *et al.*, 2011).
203 Do Lo is positioned in The Red River Delta, therefore, this place has flat topography with an
204 average elevation of 5.00m. Although located in between 2 rivers (i.e. Day River and Nhue
205 River), this area is protected from fluvial flood thanks to dike systems along these two rivers.
206 La Khe canal connects these two rivers by Yen Nghia gate (West side) and Van Phuc Gate
207 (East side). Yen Nghia pumping station, located at Yen Nghia gate, pumps water from the La
208 Khe canal to the Day River. Co Ban Chanel plays an important role in conveying the rainwater
209 and wastewater from research area to La Khe Canal. Rainwater and domestic wastewater are
210 collected by a combined sewer system (CSS) throughout the research area before discharged
211 into Co Ban canal via Southern and Western outfalls (Figure 1b). The water level in Co Ban
212 canal is under control and regulated at 5.12 m (assuming stable).
213

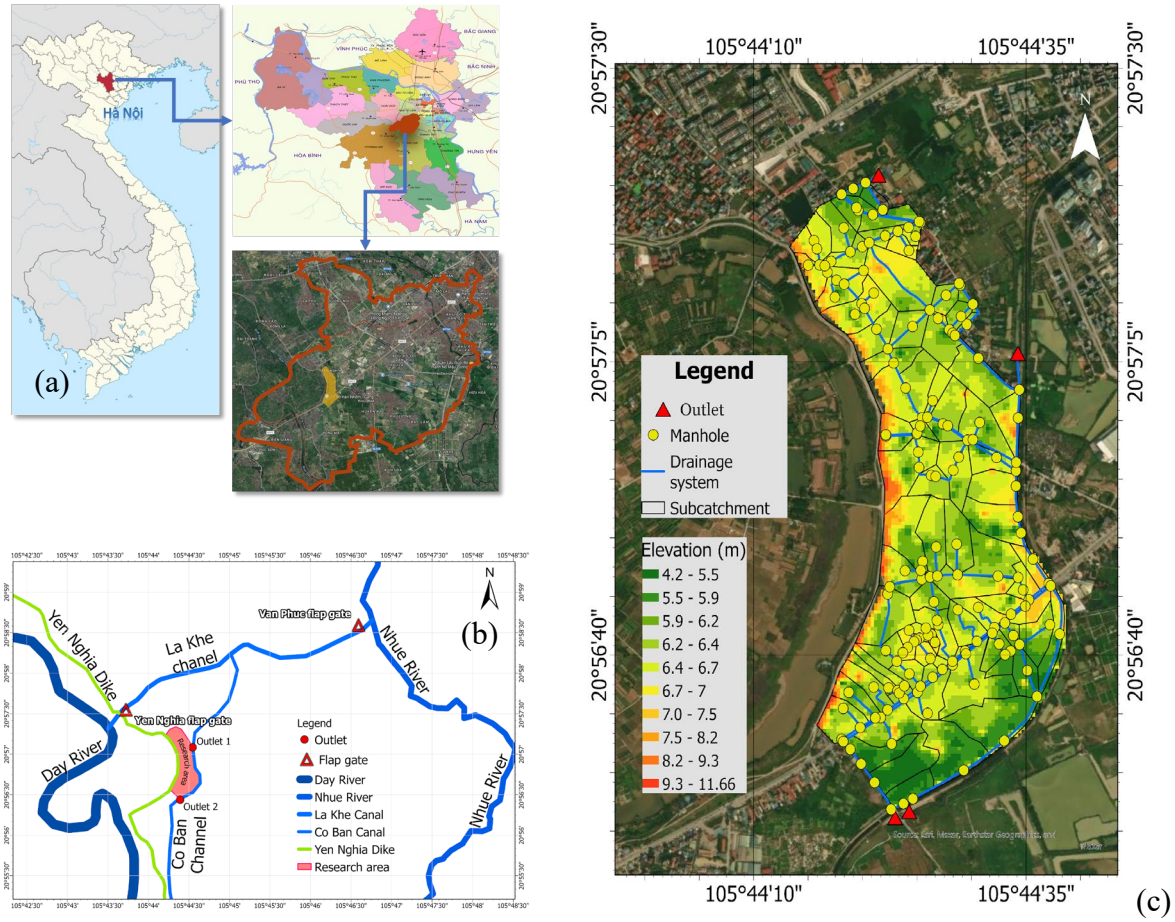

214 Figure 1. Location of the case study Do Lo – Yen Nghia Precinct – Ha Dong District – Ha Noi – Viet Nam (a); Case study hydrological connection

215 (b); Digital elevation Model (DEM), subcatchments, and drainage system (c); and landcover (d) (updated from previous research (Do Minh *et al.*,

216 2023)).

The main road Asian Highway 13 (AH13) passthroughs the case study area (Figure 1c). During the rush hour, this main road has approximated 6,000 vehicles per hour travel through. However, pluvial floods are detected frequently constraint the traffic flux in this road, according to Ha Noi Sewage and Drainage system Company (HSDC) report.

Situated on the outskirt of Ha Noi city, Do Lo District has witnessed rapid urbanization driven by the city expansion. Nonetheless, the area has received limited financial support, particularly for infrastructure development, since it is often left out in urban planning project (Luo *et al.*, 2018). As a result, the existing drainage system has struggled to keep pace with the urbanization speed. Additionally, projections indicate an anticipated increase in extreme rainfall events because of climate change. Companies who have responsibilities for flood risk management (e.g. Hanoi Drainage and Sewage system Company) are struggling to manage flood risks in this area due to the rapid occurrence of pluvial flooding and limited human resources.

MATERIALS AND METHODS

Data sources

Data used in this research were collected from several sources. To construct the framework of the drainage system model, data on the Digital Elevation Map (DEM) drainage system and land cover were collected from Ha Noi Urban Planning Institute (HUPI), Ha Noi Sewage and Drainage system Company (HSDC), and open-source Google Earth Pro, respectively. To generate the rainfall scenarios, rainfall distributions were mainly obtained from HSDC. An historical rainfall event and 47-year daily rainfall dataset from 1974 to 2020 were acquired from Viet Nam National Centre for Hydro-meteorological Forecasting (NCHMF). To evaluate fluctuations in domestic wastewater discharge, daily water supply data from January 2021 for

240 the research a was obtained from the Ha Dong Water Supply Company (HADOWA).
241 Additionally, flood extents during the rainfall events were archieved through flood data
242 collection campaigns which were specially organized in collaboration with citizens of the
243 research area.

244 **Research method**

245 In general, this study employed a systematic approach which is shown in Figure 2. This
246 approach comprises the following phases: (1) drainage network model build-up, (2) model
247 calibration and validation, (3) scenario estimation, (4) model simulation and (5) spatiotemporal
248 analysis. Firstly, the drainage network model was built based on the hydraulic data which were
249 acquired from local stakeholders including DEM, drainage system, landcover, subcatchments,
250 and dry weather condition (i.e. domestic wastewater). The data for model calibration and
251 validation (i.e. flood extent, water levels in drainage system, and the rainfall intensity) were
252 obtained from the field through flood data collection campaigns organized in 2019 and 2020.
253 The scenario estimation process utilized the statistical analysis of returned period from 47-year
254 rainfall dataset (1976 – 2020) and 3 observed storm 2008, 2019, and 2020. Flood simulations
255 were executed using SWMM. Each flood simulation outcome was analysed and interpreted
256 using spatiotemporal analysis formulas. Flood patterns, flood dynamics, as well as flood
257 expansion rate were analysed to determine the velocity of flood propagation. To specifically
258 assess the spatiotemporal changes of a flood, this study introduced the Flood Expansion Rate
259 (FER). The following parts describe in detail the step followed.

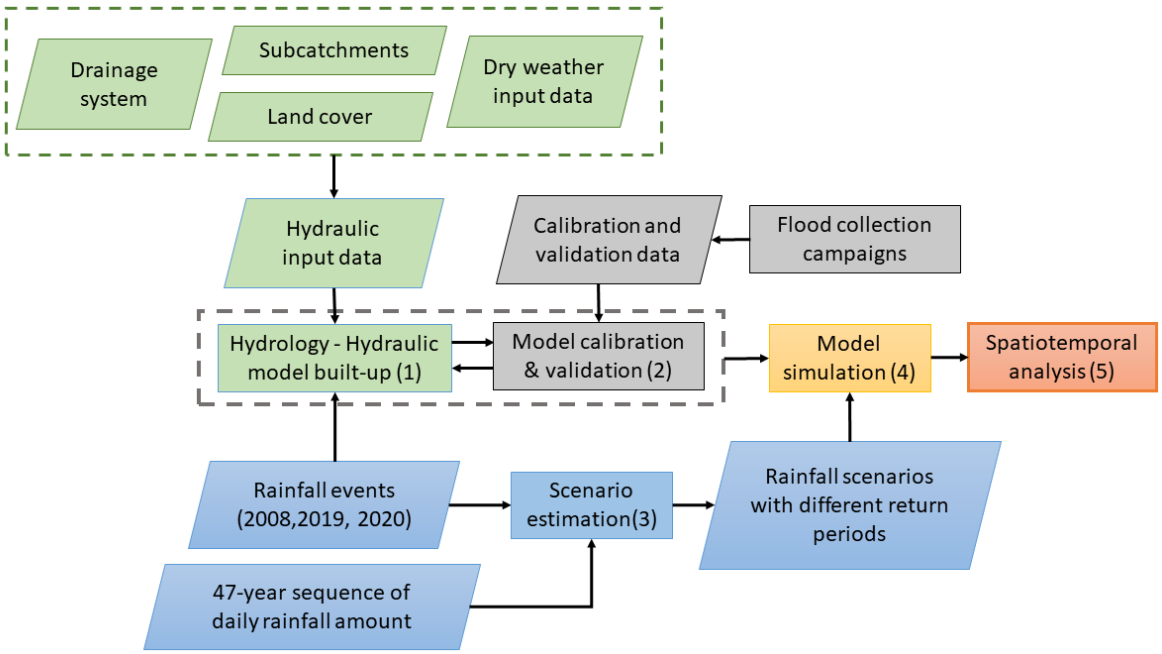

Figure 2. Research scheme

Step 1: Hydrology-hydraulic model build-up

Model Setup

To analyse effectively the diverse urban flood responses to storm events in the case study, a comprehensive drainage network model was developed. DEM, the drainage system information, the land use, landcover, the boundary conditions, and the dry weather flow data were pre-processed and integrated into the model (Figure 1).

Utilizing the 1D SWMM, the study focused on the underground drainage system as a primary determinant of urban flood locations. The model configuration included subcatchments and key nodes. Subcatchments were defined based on existing maps, with land cover data delineating pervious and impervious surfaces. Key nodes were represented for subcatchment outlets and conduit junctions. Each node in the model was assumed with a 40 m^2 ponding area above. Boundary conditions – the water levels in the outfall - were set with the Co Ban channel

marking in the eastern district boundary. This outfall water level was stably assigned a reference elevation of 5.12 m.

Urban catchment delineation

114 subcatchments were defined in this research area based on DEM, the drainage system and street pathways. DEM, sourced from the HUPI, with a resolution of 20m, played a crucial role in the model setup. VN2000 - the Viet Nam national coordinate system was used in this DEM. In order synchronize with another input data, VN2000 was transferred to WGS84 (Pham Thi *et al.*, 2019). Together with DEM, street paths and drainage system were used to delineate subcatchments and inform the hydraulic modelling, providing essential topographical insights for accurate flood simulation (Figure 1c).

Land cover

Land cover comprised by 3 types of the land: (1) Blue space consisted of pond and surface water cover; (2) Green space was made up by tree and plant cover; and (3) Urban space covered the concrete surface. Do Lo is highly urbanized area with very high percentage of concrete cover (87.34%) and low percentages of green and blue spaces (10.94% and 1.72% consecutively). Figure 1d showed the landcover map which was compiled manually from LANDSAT images on Google Earth Pro.

Estimation of Domestic Wastewater Discharge

Understanding the critical contribution of domestic wastewater, dry weather flow (DWF) was taken into account in the model. Since this area is highly urbanized, therefore, 80% of water supply amount was assumed turning to domestic wastewater. The daily water supply consumption was assumed at 300 litres per capita, based on The Vietnam national standard for water supply TCXDVN 33: 2006 Water supply – Distribution system and facilities Design Standard (Ministry of Construction of Viet Nam, 2006). Water consumption is fluctuated during the day following the household demands. This fluctuation was built based on the water

298 consumption data collected in January 2021, according to the expert's recommendation from
299 HADOWA – Ha Dong water supply company. Consequently, daily wastewater discharge
300 mirrored the water consumption pattern, providing hourly coefficients for more accurate
301 modelling. So, the amount of domestic wastewater and its daily fluctuation can be defined for
302 an individual. Meanwhile, only urban space contributed the domestic wastewater into the
303 drainage system since human lived in urban space. Green and blue space were assumed
304 providing no polluted discharge into the drainage system. DWF was calculated by daily
305 domestic wastewater discharge per capita multiplying with urban population density and urban
306 area for each subcatchment.

307 ***Step 2: Model calibration and validation***

308 In order to simulate the flood situation, five specific 24-hour rainfall distributions from
309 precipitation events were selected (i.e. Event A, B, C, D, E) (Table 1). Three of them (i.e. event
310 A, B, C) were integrated into the model build-up and calibration process. The others (i.e. event
311 D and E), meanwhile, were used for validation. Among those five rainfall distributions, four
312 of them including event A, B, D, E were obtained from HSDC on 15th October 2020, 29th
313 August 2019,5th July 2022 and 11th August 2022. These data were collected by the sensors
314 mounted nearby research area with one-minute interval. The historical event C was investigated
315 since it caused significant loss in human lives and economics in Hanoi in 2008 (Luo *et al.*,
316 2018). The heaviest rainfall day during this torrential rainfall (i.e. 31st October 2008) was
317 selected with one-hour interval. This historical data was collected from NCHMF.

318 Table 1. Five actual precipitation events in 2008, 2019, 2020 and 2022.

Rainfall event	Date of collected	Total rainfall	Usage	Resources	Resolution intervals	Equal returned

		amount (mm)				period (years)
A	15.10.2020	84.8	Input	HSDC	1-Minute	1.25
B	29.8.2019	176.6	Input	HSDC	1-Minute	5
C	31.10.2008	565.9	Input	NCHMF	1-Hour	300
D	5.7.2022	117	Validation	HSDC	1-Minute	2
E	11.8.2022	219.7	Validation	HSDC	1-Minute	10

Besides the rainfall hyetograph data, flood extent are essential data for calibrating and validating process. Flood data collection campaigns were organized during event A, D and E in order to collect the flood extent data. This data was collected by both researcher teams and also the citizens who live and work in the flood area.

Calibration and validation processes were executed to ensure that model reflected the reality accurately. Calibration process involved theoretical and empirical approaches, incorporating with expert insights. Key calibration parameters included Manning's roughness coefficients for surfaces and pipes, and infiltration rates. This process, based on trial-and-error for limited cases, was aligned with previous research and local expert recommendations. Hydraulic roughness and pipe flow coefficients were assumed based on well-established studies.

To validate the model, flood scenarios resulting from events D and E were simulated. The model results were compared with flood extent data collected by aforementioned flood data collection campaigns.

Step 3: Rainfall scenario estimation

Rainfall scenarios were used to predict future flooding. To develop these scenarios, a rainfall frequency analysis technique was deployed using the annual maximum method to estimate future scenarios. A 47-year dataset of daily rainfall amounts (1974–2020) was obtained from

the NCHMF for this analysis. The rainfall frequency analysis, detailed in Figure 3a, involved 5 steps: (1) selecting annual maximum data, (2) estimating the probability of exceedance, (3) fitting a distribution to dataset, (4) determining the 24-hour rainfall amount and (5) extrapolating the rainfall distribution patterns to rainfall scenarios. Weibull method was used to estimate the probability of exceedance. The log Pearson III distribution were used to fit the dataset according to recommendation of United State Water Resources Council (U.S. Advisory committee on water data, 1982; England *et al.*, 2019). In order to perform the Monte Carlo simulation, 7 returned period were chosen to extrapolate scenarios. The returned periods chosen are 1.25-year, 2-year, 2.5-year, 5-year, 10-year, 20-year, and 50-year. Event A, B and C were selected to derive three rainfall patterns (i.e. Pattern A, B, and C) based on its specific rainfall distribution.

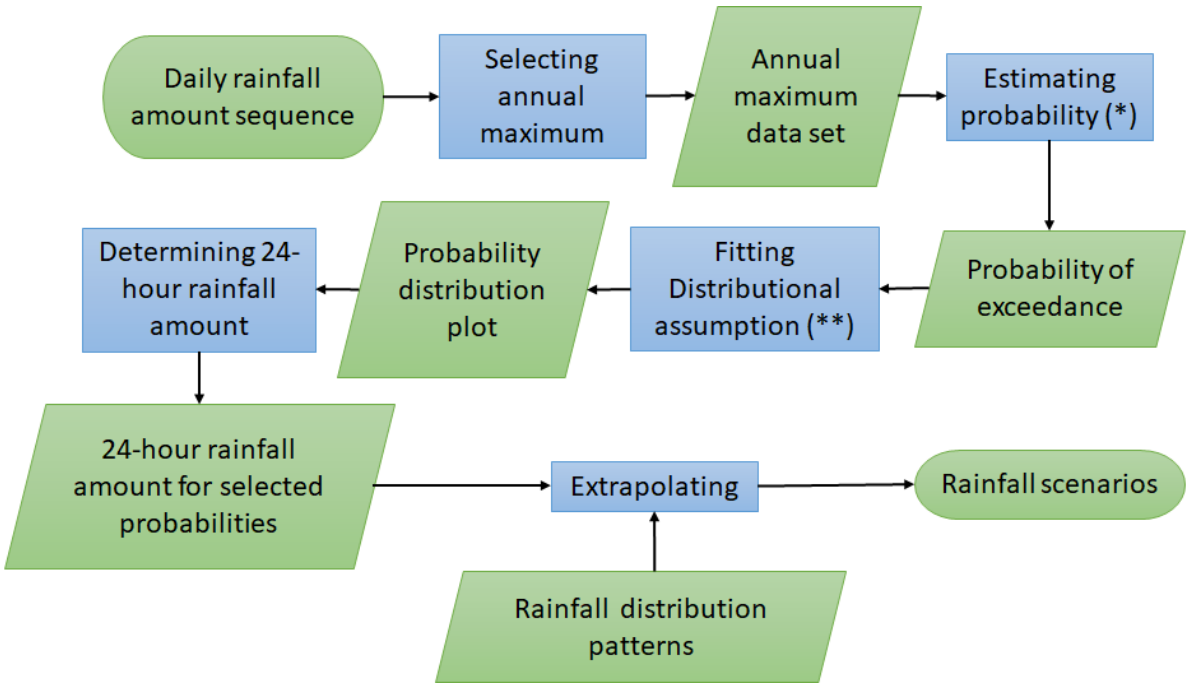

(Using the Weibull method; ** Using the logarithmic Pearson III distribution)*

(a)

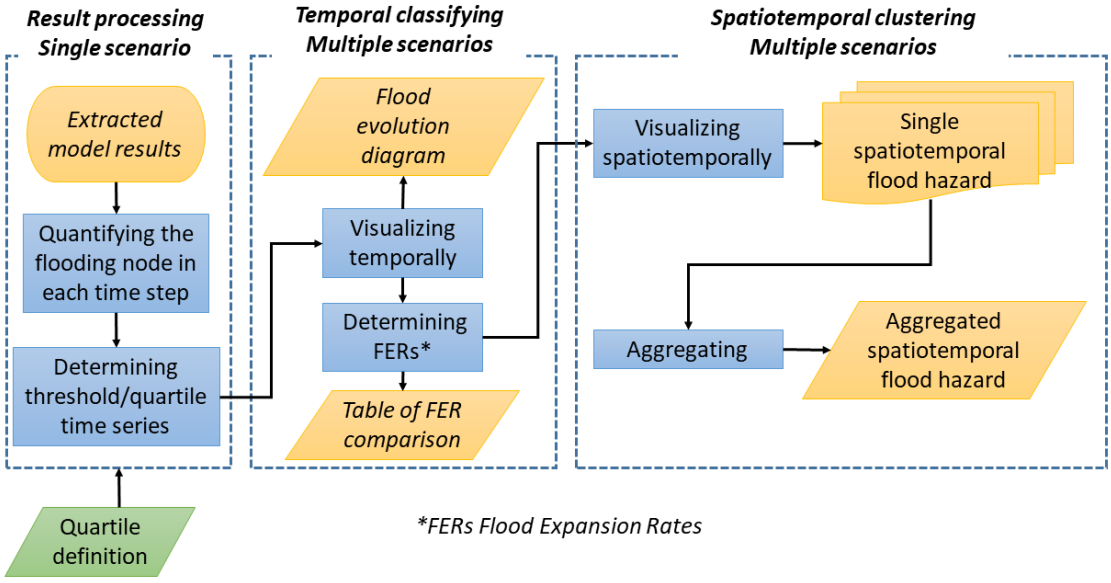

(b)

348 Figure 3. Detailed methodologies of (a) rainfall frequency analysis and (b) PNFA

349 ***Step 4: Model simulation***

350 24 rainfall scenarios were used to simulate the flood scenarios for this case study. Among these
351 scenarios, 21 synthetic rainfall scenarios constructed by 3 rainfall patterns and 7 returned
352 periods. The other 3 rainfall scenarios were the actual rainfall events – Event A, B, and C. The
353 Monte Carlo simulations were designed using daily rainfall amounts. The total rainfall volume
354 was adjusted while the rainfall hyetograph shape was maintained, based on observed events.
355 This approach ensured long-term statistical reliability; however, we recognized that the use of
356 daily data may under-represent short-duration peak rainfall intensities, which are critical in
357 certain extreme events.
358 Flood simulations were run by SWMM, manipulated and extracted by tailor made python script
359 using SWMM_api package (Pichler, 2022). Although the rainfall data were collected in 24-
360 hour span, the flood simulation covered 72-hour span, including 24-hour before the rainfall
361 event, 24-hour of rainfall event, and 24-hour after the rainfall event. The extended span ensured

362 to stabilize the domestic wastewater setting in the drainage system and also captured fully the
363 flood after the rainfall (if available).

364 ***Step 5: Spatiotemporal analysis using Percentage of Node in Flood Assessment (PNFA)***

365 Flood analysis was conducted based on the modelling results obtained in Step 4. While
366 conventional flood analysis primarily considers the spatial distribution of flood hazards, this
367 study incorporated the temporal dynamics of flood hazards. Flood-related data were extracted
368 at discrete time steps and processed using the Percentage of Node in Flood Assessment (PNFA)
369 method. This approach evaluated flood risk based on predefined thresholds of node inundation.
370 The expected outcomes of this analysis included the Flood Expansion Rate(s), Temporal flood
371 expansion patterns, and a Spatiotemporal flood hazard map.

372 **Percentage of Node in Flood Assessment (PNFA)**

373 **The Percentage of Node in Flood Assessment (PNFA)** is a novel assessment approach for
374 analysing urban flood dynamics over both space and time. PNFA concerns not only the spatial
375 flood hazard but also the temporal flood hazard.
376 To incorporate the temporal scale into flood analysis, flooding time steps were thoroughly
377 examined in each scenario, before being aggregated to get a comprehensive analysis of the
378 spatiotemporal flood evolution. The spatiotemporal flood evolution was presented in 3 forms:
379 diagram expression (Temporal flood Expansion), numerical expression (Flood Expansion rate
380 - FER), and map expression (Spatiotemporal flood hazard maps). The spatiotemporal flood
381 quartiles were defined to assist the temporal flood analysis. Figure 3b showed spatiotemporal
382 flood analysis step by step: (1) Flood result processing in a single scenario, (2) Temporal
383 classifying in multiple scenarios, and (3) Spatiotemporal clustering in multiple scenarios.

Spatiotemporal flood quartile definition

To clarify the flood evolution spatiotemporally, flooded nodes were classified into 4 quartiles based on the flood sequence in time (Figure 4).

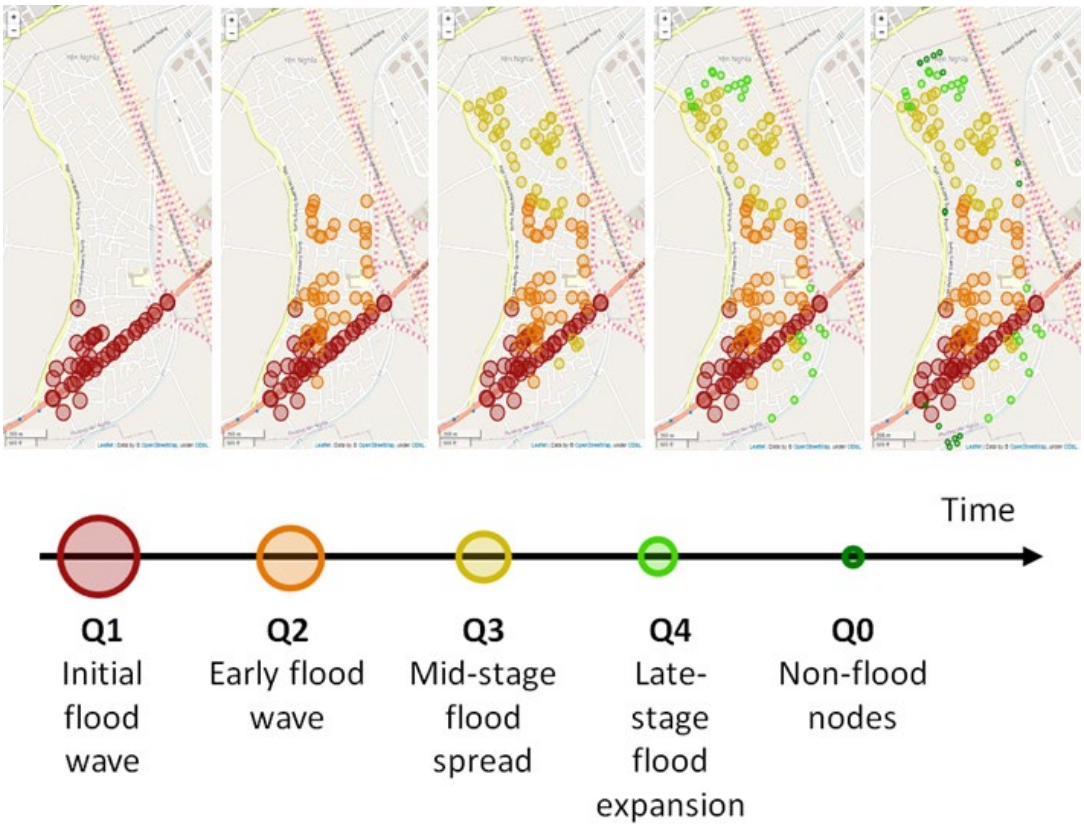

Figure 4. Illustration of flood evolution process during the flooding time

These spatiotemporal quartiles were introduced in order to classify the magnitude of flood risk based on the time scale. These spatiotemporal quartiles included four main quartiles (i.e. Q1, Q2, Q3, Q4) and one extra quartile Q0 for non-flood manhole.

- Q1 (Initial flood wave): Represented the first quartile (0 – 25%) nodes in flood, encompassing the first 42 flooded nodes. This quartile captured the initial impact of flood.
- Q2 (Early flood propagation): Constituted the second quartile (25-50%) nodes in flood, including flooded nodes from 43rd to 84th. These nodes flooded subsequently to the initial wave, marking the early stages of flood propagation.

- Q3 (Mid-stage flood spread): Encompassed the third quartile (50-75%) nodes in flood, from flooded nodes from 85th to 126th. This group indicated nodes that flooded during the mid-stage of the event.
- Q4 (Late-stage flood expansion): Included the final quartile (75-100%) nodes in flood, indicating the percentage of nodes that were the last ones experiencing the flood.
- Q0 (Non-flooded nodes): This category was reserved for nodes that did not experience flood during the event which were outside of the quartile classification.

Due to variations in scenario conditions, the distribution of nodes across these classifications could be differed. In some scenarios, there were no node falling into Q3 or Q4 categories. Those events might have more concentrated floods or just being less intensive flood events. Conversely, some other scenarios, with broader flood impacts, have nodes distributed across all four quartiles. Across the scenarios, several nodes, that remained unaffected by flooding, were consistently classified as Q0, providing a clear distinction between flooded and non-flooded regions within the model simulations. The flood with less than 25% of node in flood were not considered as critical condition.

This quartiles definition was initial but essential step for spatiotemporal analysis, which gave thresholds to determine the flood propagation speed in later phrase.

Spatiotemporal analysis

The spatiotemporal analysis focused on both the temporal and spatial distributions of floods by 3 consecutive stages including: result processing, temporal classifying, and spatiotemporal clustering.

Firstly, result processing was applied for each scenario simulation to understand the flood situation through each time step. Flooding data was extracted from the simulation results. The number of flooding nodes in each time step was tracked down. When the number of flooded

nodes reached certain quartile thresholds, the time periods were recorded. Those incremental time series represent the flood evolution during the flooding time.

Secondly, temporal classifying focused only on the temporal scale of floods, assessing the agility and rapidity of the flood extension. Flood evolution time series of various scenarios were charted to illustrate the flood expansion speed. This expansion speed was also calculated numerically by FER.

Lastly, spatiotemporal clustering provided a deeper analysis of the previous stage by considering both the temporal and spatial distribution of floods across all scenarios. Individual spatiotemporal flood distributions were clustered and visualized geographically using prior classifications and key node locations. The aggregated spatiotemporal flood distribution was constructed by overlaying all individual distributions, providing a comprehensive view of spatiotemporal flood hazards. This analysis identified two key types: the most critical spatiotemporal flood hazard, and the highest potential spatiotemporal hazard.

Flood expansion rate (FER)

In order to compare numerically the flood agility and rapidity during the temporal classification, FER was introduced in formula (1).

$$\mathrm{FER_{ij}} = \tan \alpha_{ij} = \frac{\Delta \mathrm{PNF_{ij}}}{\Delta \mathrm{FEI_{ij}}} = \frac{PNF_j - PNF_i}{FEI_j - FEI_i} \quad (1)$$

Where i, and j are threshold of Percentage of Node in Flood reach at the certain quartile (e.g. 25%, 50%).

FER_{ij} is the flood expansion rate (FER) from threshold i to threshold j.

FEI_{ij} is Flood Evolution Interval from threshold i to threshold j.

α_{ij} is the angle (rad) between flood evolution slope during flood evolution FEI_{ij} and time axis.

PNF_{ij} is Percentage of Node in Flood from threshold i to threshold j.

In this research, we considered threshold i at zero minute when the induced rain started.

Percentage of Node in Flood at moment j PNF_j is calculated by the formula (2) below.

$$PNF_j = \frac{NNF_j}{TN} x100 \quad (2)$$

Where NNF is the Number of Nodes in Flood at threshold j.

TN is the Total number of Nodes in drainage system in the considered assessment.

RESULTS

Modelling results

Drainage network model build-up

Model was built-up based on the urban subcatchments, land cover, domestic wastewater estimation. There are 114 subcatchments were divided based on the drainage system and DEM map. The results indicate that the case study area is predominantly covered by concrete, accounting for 87.34% of the total surface. Only 10.94% of the area is covered by vegetation, while water surfaces occupy 1.72%. The total domestic wastewater used in this research was 2,489.52 m³ per day, distributed across 114 subcatchments. The discharge fluctuations throughout the day followed the domestic wastewater discharge pattern, which closely mirrored the water supply demand data collected from HADOWA between January 4 and January 31, 2021. This period was recommended by experts as it closely resembled the observed period.

Model calibration and validation

During the flood data collection campaigns, residents of AH13 were asked to report flood extents during events A, D, and E. Flood extent data were gathered by both local citizens and

464 workers living and working in the study area. The reported flood extents for events A, D, and
465 E closely matched the model results, indicating that the developed model effectively replicated
466 the hydraulic system and flood conditions in the area (Figure 5).
467

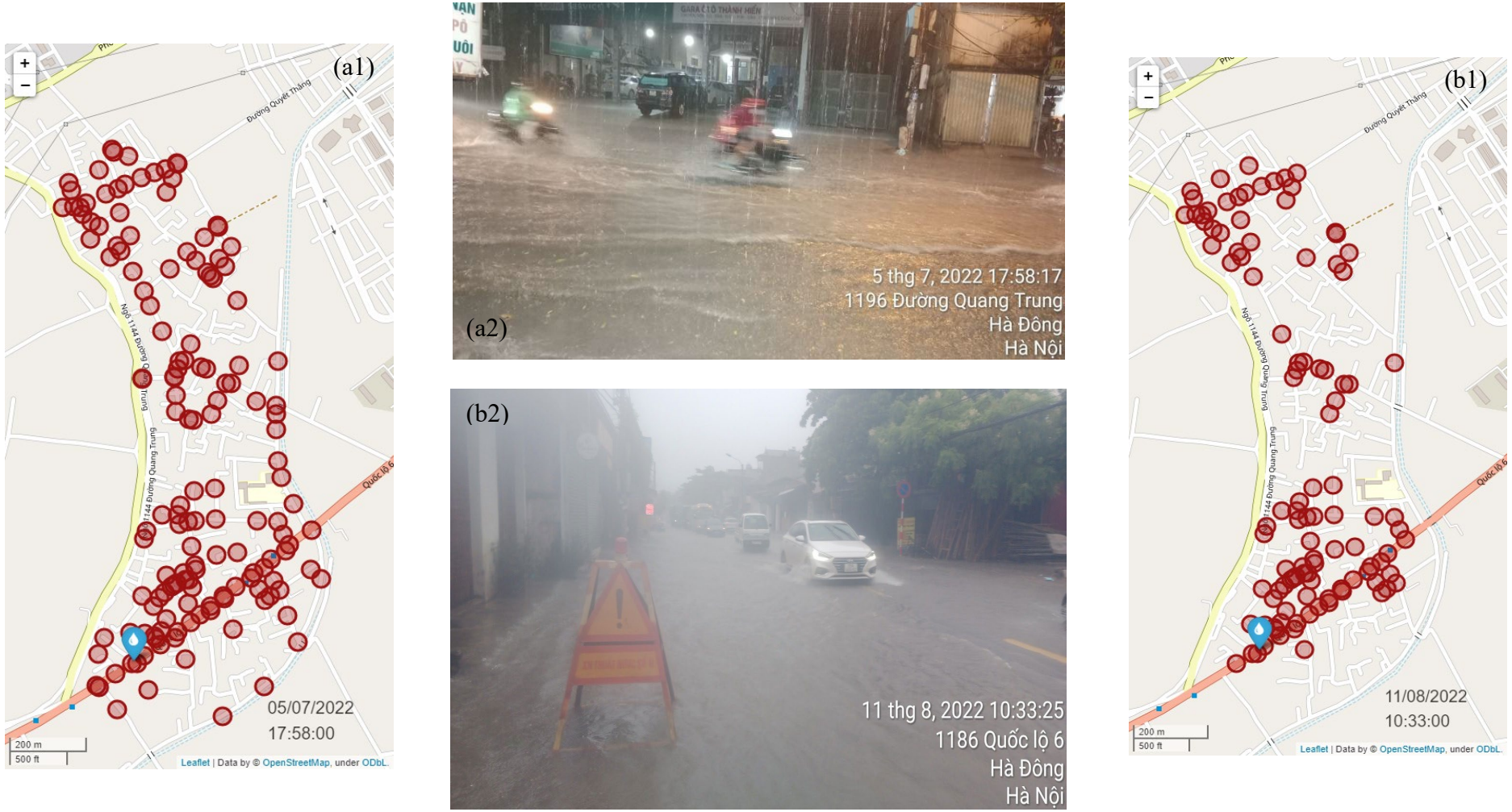

Figure 5. Flood extent in model and in the field during event D (a1, a2) and event E (b1, b2)

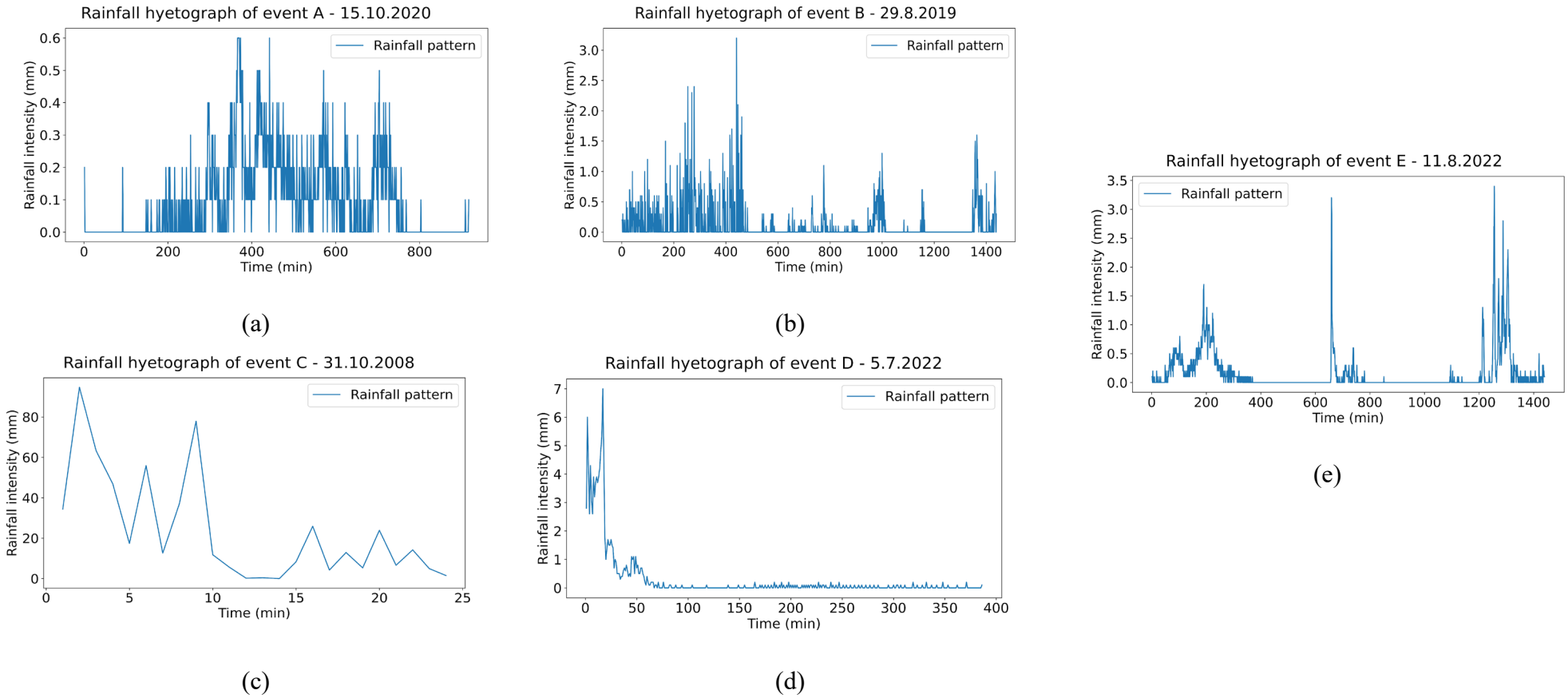

Figure 6. Actual rainfall distributions in event A (15.10.2020) (a), event B (29.8.2019) (b), event C (31.10.2008) (c), event D (05.07.2022) (d), and event E (11.8.2022) (e)

Rainfall patterns and rainfall scenarios.

6 showed the 5 actual rainfall hyetographs used in the research. Event A, B, and C were used to build and calibrate the model while event D and E were used to validate the model. Event A, B and C were used to create the temporal distribution pattern of the rainfall namely pattern A, B and C, consecutively. Those patterns were used as the baseline to extrapolate to different returned period rainfall scenarios later.

Rainfall frequency analysis was executed. 7 chosen returned period scenarios and their daily rainfall amount are shown in Table 2 below. Rainfall patterns (i.e. pattern A, B, and C) were extrapolated throughout 7 return period scenarios. the temporal distribution of the rainfall patterns remained unchanged, the intensity of these patterns was modified into 21 scenarios with 1-minute and 1-hour intervals.

Table 2. Daily rainfall amounts are equivalent of the chosen returned periods.

Returned period (year)	Daily rainfall amount (mm)
1.25	86.91
2.0	117.69
2.5	133.88
5	188.32
10	246.91
20	308.69
50	394.52

Model simulation

A total of 21 previously mentioned rainfall scenarios, along with 3 actual rainfall events, were used as input rainfall to simulate the calibrated model, resulting in 24 scenarios in total. For each scenario, the time sequence of flooding at each node was extracted using custom Python code based on the SWMM_api library. These results were then pre-processed for subsequent spatiotemporal flood analysis.

Spatiotemporal flood analysis using PNFA

Result processing for single scenario

A flood assessment period was set in each simulation. The beginning of this period was the moment that rainfall started. The assessment period concluded either at the time of the last recorded rainfall or when the final flood of the entire region subsided. Flood results from the simulation were extracted into a timeline table recording data every minute for every key manhole in the system.

The flood situation of event A was examined thoroughly by 3 represented nodes N31-17-1, N10-17-1 and N11-46 as a detailed illustration. Those node's locations were shown in Figure 1c. In this flood event, some node got flood in early stage of the rain such as Node N31-17-1 (Figure 7b). Node N31-17-1 experienced the lag time/lapse time between the initial rainfall and initial flood so-called Lag Interval (LI) at 191 minutes. As can be seen in Figure 7b, this node also encountered longer flood duration during the assessment period. The surface area on top of this node also was the most vulnerable area with flooding in this area. Simultaneously, some other nodes like N10-17-1 experienced the flood later, and also had a shorter duration of flood (Figure 7c). The LI of node N10-17-1 was 370 minutes. The surface area on top of this node was less vulnerable to flood comparing with node N31-17-1. Meanwhile, several nodes,

507 for example N11-46, had no flood during the assessment period. This node did not have the LI
508 (Figure 7d).
509 To gain a broader perspective on the flood evolution during the flooding time, the Number of
510 Nodes in Flood (NNF) was recorded every time step. Figure 7e showed the dynamics of NNF
511 during the flooding time. The Flood Evolution Intervals (FEIs) that flood area reached the
512 certain thresholds based on percentage of node in flood (PNF) were defined. As
513 abovementioned, those thresholds include Q1 25% (~42/167 nodes in flood), Q2 50% (84/167
514 nodes in flood), Q3 75% (126/167 nodes in flood), Q4 over 75% (over 126/167 nodes in flood),
515 and Q0 – non-flood quartile (non-flood nodes). In case of event A, the maximum NNF were
516 101 nodes ~ 60.5% PNFs, which was smaller than 75% (Q4). Therefore, in this case, only Q1,
517 Q2, Q3 and Q0 thresholds were considered. There was no node belonging to Q4 threshold
518 (above 75% node in flood). The LI in whole area are 191 minutes (Figure 7e).

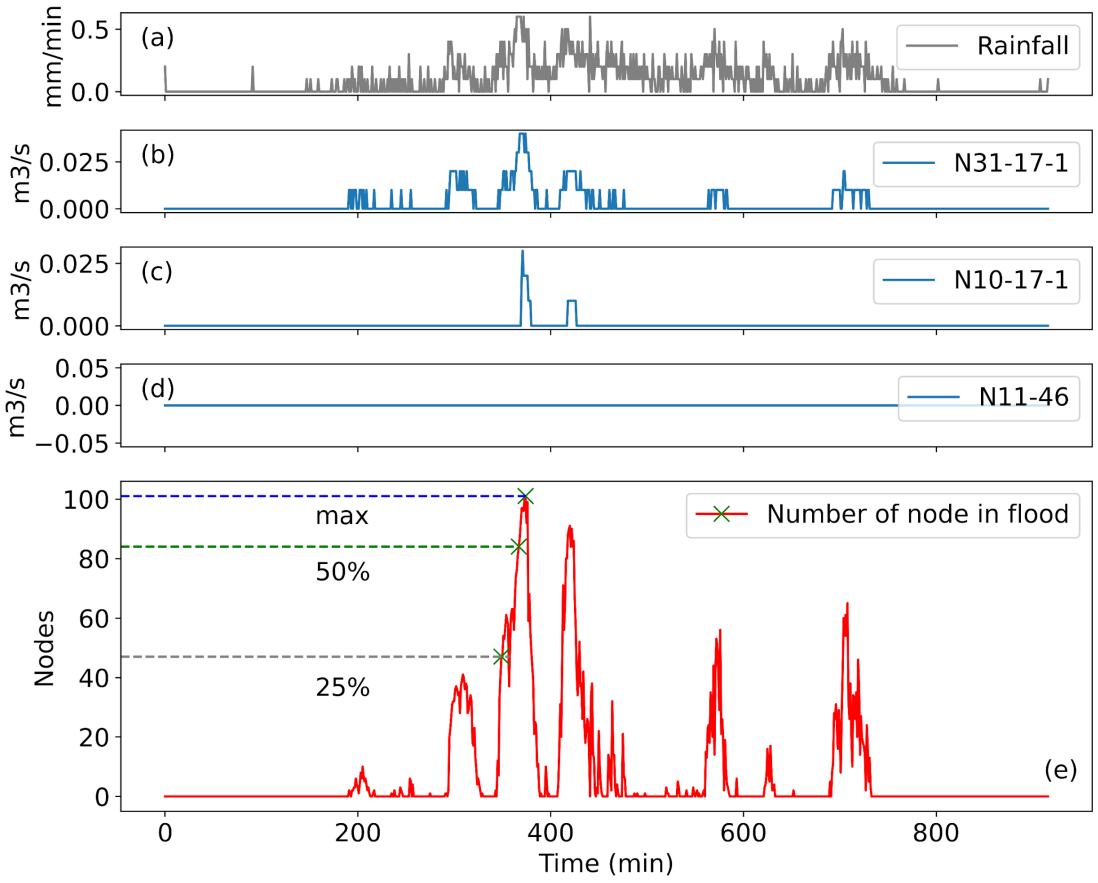

Figure 7. Flood simulation result extractions from event A: Rainfall distribution (a); Flooding dynamics in node N11-1 (b), N10-17-1 (c), node N11-46 (d); and the number of nodes in flood (e).

As flood quartile definition, $FEI_{25\%}$ was the duration when flood area reached 25% PNF ~ NNF = 42 nodes in flood. In fact, depending on the rainfall intensity and flood situation, the NNF was not always accurate at 42 nodes. As a consequence, to capture real situation, the very first moment when the PNF was over 25% would be selected to be the first threshold ($FEI_{25\%}$), PNF was also re-calculated to fit with updated selection. So, in case of the event A, the selected PNF and FEI were showed in Table 3. The similar process was applied for another 23 scenarios.

Table 3. NNF, PNF and FEI of flood simulation in event A

NNF (nodes)	PNF	FEI (min)

47	28.14 %	349
84	50 %	367
101	60.5 % (max value)	374

Temporal classification for multiple scenarios

To analyze the temporal flood evolution, a temporal flood expansion diagram was built. Each line in the graph reflects the process that the flood rose from zero to maximum number of nodes in flood through the timeline. There were 3 important temporal flood factors needed to consider: Percentage of Node in Flood (PNF), Flood Evolution Interval (FEI) and Lag Interval (LI). Those factors were defined in previous process.

Figure 8a depicts the flood evolution of three actual rainfall events: A, B, and C. Event A was the least severe in terms of temporal scale, with the lowest maximum PNF (64%), the longest maximum FEI (376 minutes), and the longest LI (107 minutes). Event C was the most severe, with the highest maximum PNF (89%), the shortest maximum FEI (95 minutes), and the shortest LI (2 minutes). Event B was a moderate event, with an average PNF (72%), FEI (282 minutes), and LI (5 minutes). These flood reactions reflect the intensity and amount of rainfall for each event. Since the three rainfall events (A, B, and C) had different returned periods (1.25-year, 5-year, and 300-year, respectively), it was difficult to pinpoint the differences between the three rainfall patterns.

Figure 8b, c, and d show three comparisons of different rainfall patterns across different scenarios. From these diagrams, it is evident that more intense rainfall results in a higher PNF. However, rainfall intensity seemed to have a lesser effect on the FEI in pattern C (70–149 minutes), but not in patterns A (373–376 minutes) and B (282–284 minutes).

The results show that pattern A, with low returned periods (1.25-year, 2-year), exhibits a long LI (~100 minutes), which corresponds to a decrease in rainfall intensity. This extended LI is

547 due to the intermittent rainfall at the start of the assessment period. However, when the rainfall
548 intensity increased, the flooding caused by pattern A occurred almost immediately after the
549 rain began. The limited capacity of the drainage system is believed to be the primary cause of
550 this phenomenon.

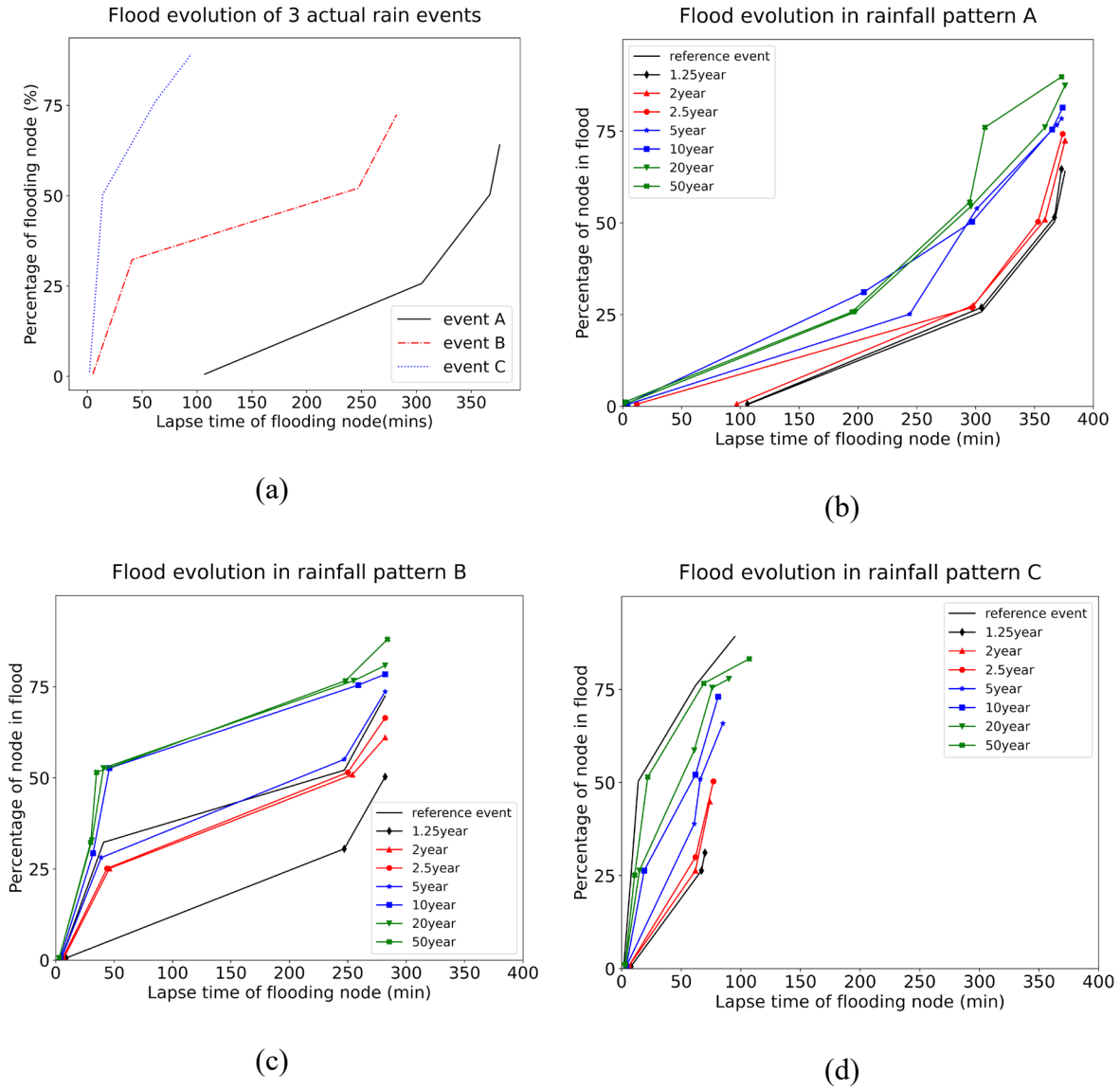

Figure 8. Temporal flood expansion: Comparison of three actual events A, B, C (a); with each flood pattern representing different scenarios Event A (b), Event B (c), and Event C (d).

551 To numericaly quantify the flood extent spreading speed, FER was calculated as shown in
552 Table 4. Pattern A caused the largest flood areas; however, FERs of pattern A were the lowest

553 number comparing with the others. Time for flood preparation/evacuation in pattern A was
554 longer than the other patterns (i.e. patterns B, C).

555 Table 4. Flood expansion rate (FER) of 3 rainfall distribution patterns in different scenarios.

Scenario	Scenario number	Event A	Event B	Event C
Actual event	0	0.170	0.257	0.939
1.25-y RP*	1	0.173	0.178	0.445
2-y RP	2	0.193	0.217	0.607
2.5-y RP	3	0.199	0.236	0.653
5-y RP	4	0.210	0.261	0.775
10-y RP	5	0.218	0.278	0.902
20-y RP	6	0.233	0.287	0.865
50-y RP	7	0.241	0.310	0.778

556 **y RP: year Returned Period*

557 ***Spatiotemporal clustering (individual scenario visualization)***

558 Flood quartiles combined with location showed the spatiotemporal distribution of the flood. In
559 Figure 9a, flooding node locations during event A were shown for different time scales. During
560 these events, the initial areas experiencing flood were divided into three centres, concentrated
561 mostly in the main road AH13 and adjacent regions. Subsequently, the flood gradually
562 extended to the surrounding section of the road and then spread towards the northern part of
563 the area. Notably, the regions near the Northern and Southern outfalls remained unaffected by
564 floods across the various scenarios. Based on the spatiotemporal flood node locations, a
565 spatiotemporal flood hazard map was generated using the Inverse Distance Weight (IDW)
566 interpolation method (Figure 9b). This flood hazard map provides an initial overview of how
567 the flood evolved spatially and temporally during the actual rainfall event A. Flood regions

were categorized following temporal flood quartiles (i.e. Q1, Q2, Q3, Q4, and Q0). This spatiotemporal flood distribution gives a different view on flood evolution and flood prevention priority. This complemented the spatial flood distribution which was built up based on the total flood discharge in each node (Figure 9c). Comparing with spatial distribution, the vulnerable areas were enlarged around the main street AH13. Flood areas were concentrated in 3 areas across the study area. Continuously, the other 23 single flood hazard maps were generated for other 23 rainfall scenarios, create a data set of flood hazard maps (Figure 10a, and b).

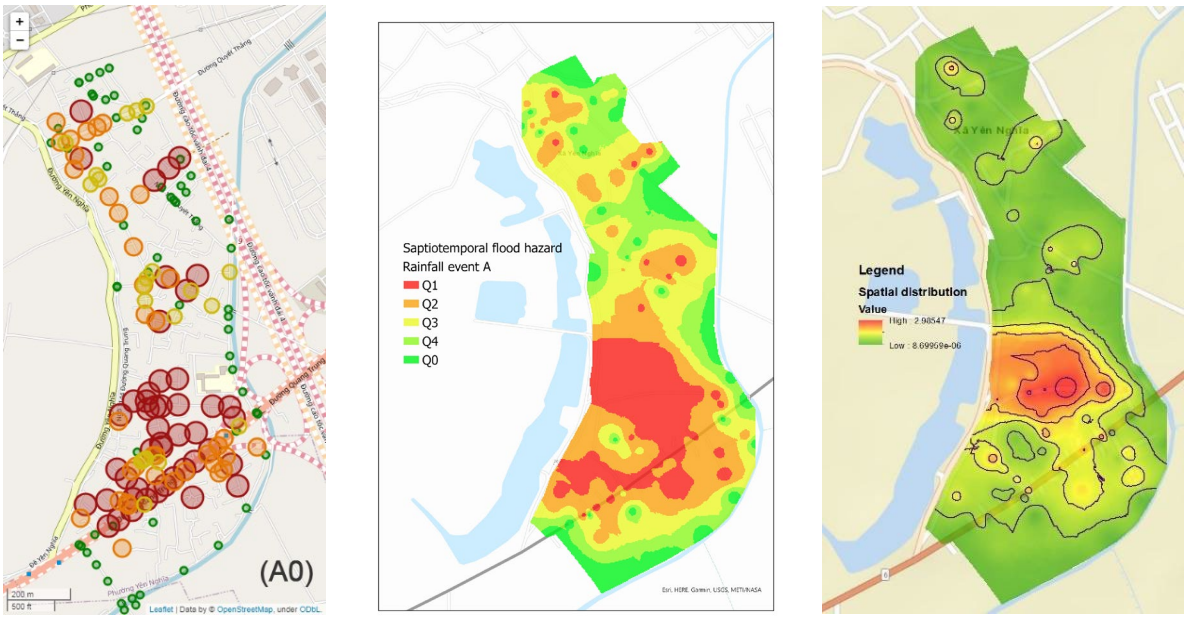

(a) (b) (c)

Figure 9. Historical event A: (a) Spatiotemporal flood node locations, (b) Spatiotemporal flood distribution, and (c) Spatial flood distribution.

Figure 10a illustrates the temporal evolution of the flood-affected area under the temporal scale. The results indicate that rainfall intensity significantly influences the rate of flooding. Specifically, Pattern A resulted in the slowest flood progression, with flooding occurring between 195 and 376 minutes. In contrast, Pattern C induced a flash flood within a much shorter timeframe, ranging from 8 to 107 minutes. Pattern B produced an intermediate flooding response, with flood onset occurring between 30 and 284 minutes. Furthermore, when

581 comparing the three rainfall patterns under the same returned period scenario, it is evident that
582 mild rainfall (Pattern A) led to a slower flood spread over a larger area compared to torrential
583 rainfall (Pattern C). These findings highlight that the temporal distribution of rainfall, or the
584 shape of the rainfall hyetograph, plays a crucial role in determining flood timing on the ground.
585 However, although the induced rainfall varies in pattern and intensity, the flood evolutions
586 exhibit a similar pattern across all 24 scenarios under the quartile scale (Figure 10b). Regions
587 nearby the outfalls, have never experienced flooding. There are some flooding nodes which
588 swing between 2 quartile ranks (e.g. from Q2 to Q3 and vice versa). Those flexible-in-rank
589 nodes created the slightly differences between various scenarios. Nevertheless, in brief, flood
590 in the research area evolved in certain pattern. This means that the spatiotemporal flood
591 analysis is stable and reliable to use in flood risk assessment.

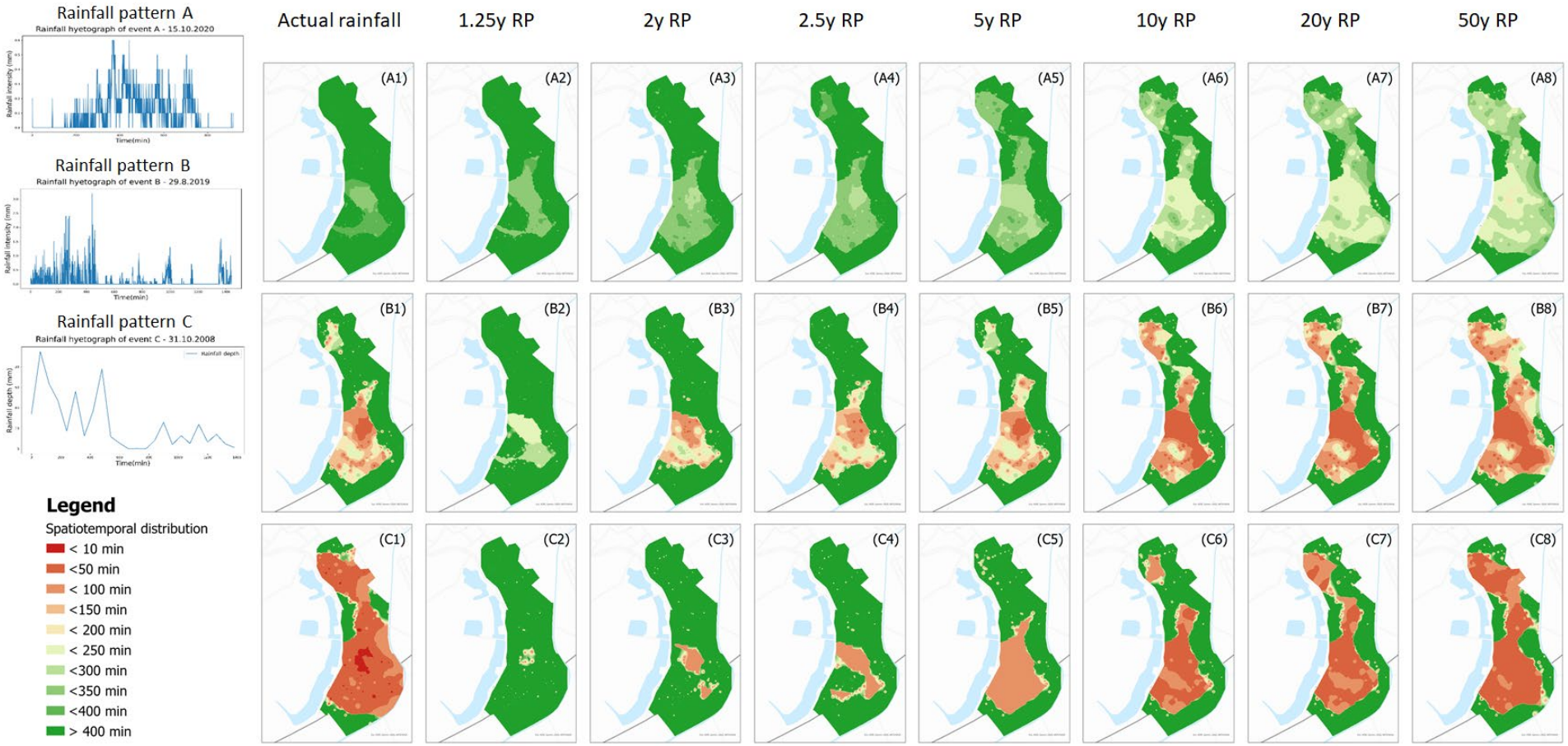
Rainfall pattern A
Rainfall hyetograph of event A - 15.10.2020
Rainfall pattern B
Rainfall hyetograph of event B - 29.8.2019
Rainfall pattern C
Rainfall hyetograph of event C - 31.10.2008
Legend
Spatiotemporal distribution
< 10 min
<50 min
< 100 min
<150 min
< 200 min
< 250 min
<300 min
<350 min
<400 min
> 400 min
Actual rainfall
1.25y RP
2y RP
2.5y RP
5y RP
10y RP
20y RP
50y RP
(A1)
(A2)
(A3)
(A4)
(A5)
(A6)
(A7)
(A8)
(B1)
(B2)
(B3)
(B4)
(B5)
(B6)
(B7)
(B8)
(C1)
(C2)
(C3)
(C4)
(C5)
(C6)
(C7)
(C8)

(a)

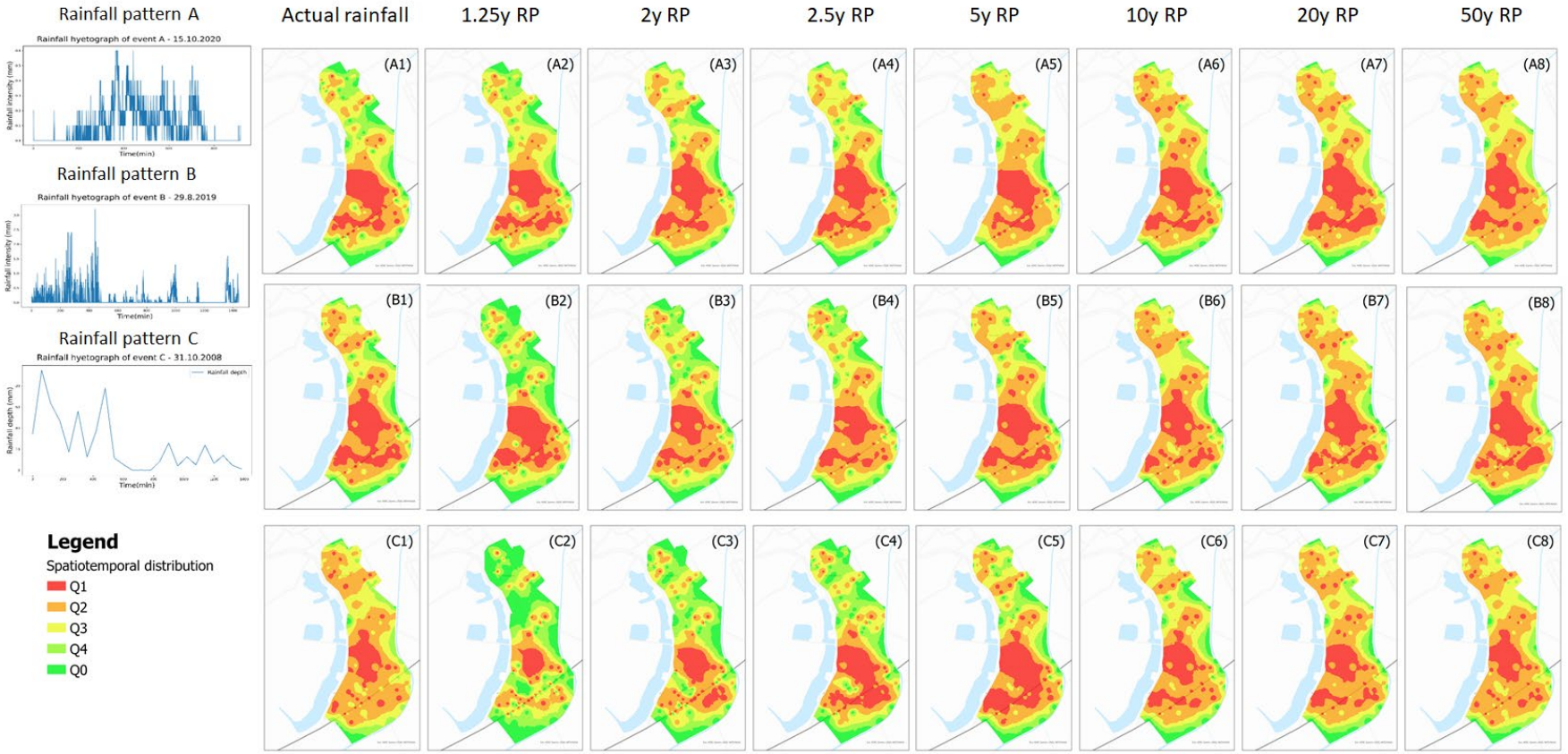

(b)

Figure 10. Spatiotemporal flood hazards in 24 scenarios of 3 rainfall patterns (i.e. A, B, C) with 8 scenarios (i.e. 1,25-year, 2-year, 2,5-year, 5-year, 10-year, 20-year, 50-year returned period, and actual rainfall distribution) with time scale (a) and with quantile scales (b) *(y RP: year Returned Period).*

For more details, although the main spatiotemporal flood pattern remained unchanged, there were still slight differences in flood distributions caused by different rainfalls. In terms of flood area, rainfall pattern A had the largest affected area compared to the other patterns within the same returned period scenarios whereas rainfall pattern C with the same returned period scenario, caused flooding in the smallest area. The flood simulation results from rainfall pattern C were contrary to expectations based on the historical rainstorm data. For example, within the 1.25-year returned period, pattern C caused flooding in a total of 52 nodes, approximately 31% of the observed nodes in the research area. Meanwhile, pattern B and pattern A caused flooding in 84 nodes (~50.3%) and 108 nodes (~64.7%), respectively. More details are shown in Table 5. This trend was consistent across other scenarios (Figure 10b). Rainfall intensity is believed to be the primary factor driving this phenomenon. In fact, rainfall pattern A had a milder intensity compared to rainfall pattern C. In conclusion, the same amount of rainfall over a shorter period resulted in a more concentrated flood area than when it occurred over a longer period. Consequently, the spatiotemporal flood hazard maps also reflect these slight differences.

Table 5. Maximum number of nodes in flood caused by 3 rainfall patterns and 7 scenarios

Scenarios	Pattern A		Pattern B		Pattern C	
	N (nodes)	%	N (nodes)	%	N (nodes)	%
1.25y RP*	108	64.67 %	84	50.3 %	52	31.13 %
2y RP	121	72.46 %	102	61.08 %	75	44.91 %
2.5y RP	124	74.25 %	111	66.47 %	84	50.3 %
5y RP	131	78.44 %	123	73.65 %	110	65.87 %
10y RP	136	81.44 %	131	78.44 %	122	73.05 %
20y RP	146	87.43 %	135	80.84 %	130	77.84 %

50y RP	150	89.82 %	147	88.02 %	139	83.23 %

615 ** y RP: year Returned Period*

616 ***Aggregated spatiotemporal flood distribution***

617 In the previous step, flood distributions were examined throughout 24 different scenarios.
618 Similar spatiotemporal flood patterns were found across various scenarios. The spatiotemporal
619 flood hazard evolution remained stable throughout the different scenarios. In addition, the
620 flood-affected areas among the 3 rain patterns differed slightly, despite being simulated under
621 the same returned period. Therefore, in order to get a holistic view on the flood evolution, flood
622 distributions during 24 scenarios were overlaid and aggregated to created a spatiotemporal
623 flood hazard map.
624 Figure 11a shows the most critical spatiotemporal hazard and its associated probabilities.
625 Flooding at each node can vary across different categories of spatiotemporal distribution. The
626 most critical situation corresponds to the fastest flood category, which is the most likely to
627 occur across all 24 scenarios. The probability of this critical situation is also depicted on the
628 map.
629 Similarly, the high-potential spatiotemporal flood hazard is presented in Figure 11b. Its
630 probability is also shown in this map. These two maps highlight the vulnerable locations in
631 research area where experienced flood spatially and temporally, as well as the potential flood
632 evolutions. These maps can be valuable for stakeholders, such as drainage system companies,
633 in maintaining the drainage infrastructure and optimizing the allocation of human resources
634 during flooding events. They can help address the issue of human resource shortages during
635 such times. On the other hand, these two maps can serve as an initial foundation for
636 implementing nature-based solutions, as they identify temporally sensitive areas.

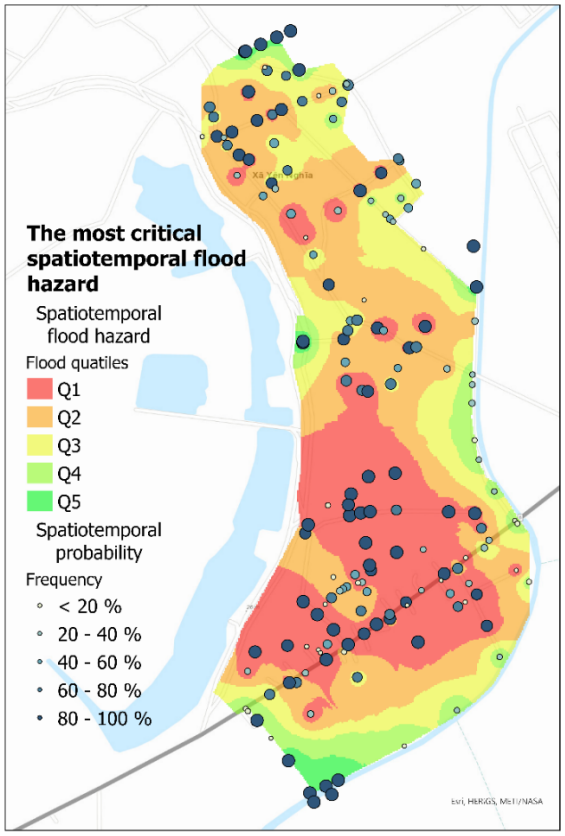

(a)

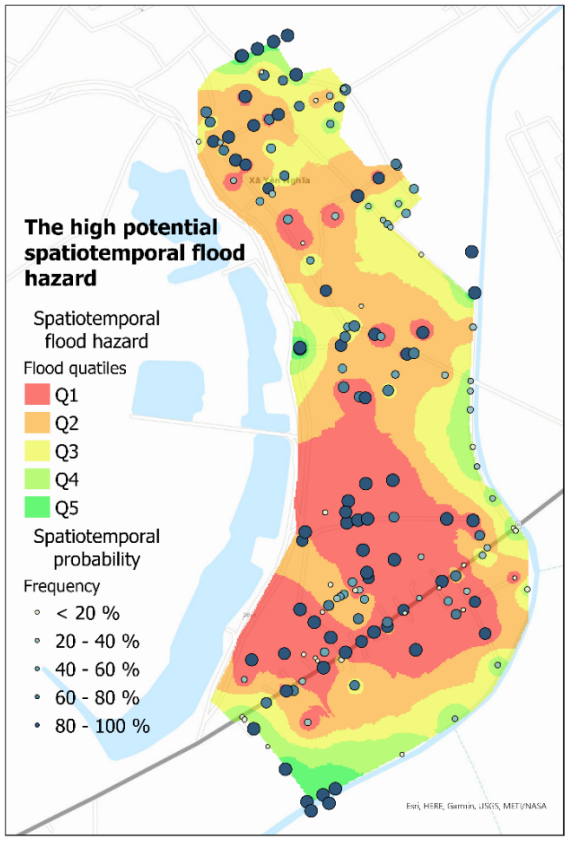

(b)

Figure 11. Aggregated spatiotemporal flood hazard: (a) The most critical spatiotemporal flood hazard, and (b) The most probable spatiotemporal flood hazard

637

DISCUSSION

Temporal Analysis

Temporal flood analysis is the initial step to characterize the flood hazard in the area. The FER serves as an initial and straightforward coefficient for gauging flood propagation speed or agility, offering a numerical basis for comparing flood dynamics across varying time scales. During one rainfall event, the flood risk to pedestrians is different over time during the rainfall event (Corzo Perez *et al.*, 2024). The FER, which represents flood severity, was used to quantify the magnitude of the flood over time during the rainfall event. Additionally, FER serves as a global indicator that allows for the comparison of flood speeds across various events, regardless of rainfall duration. The higher the FER, the faster and more dangerous the flood, irrespective of the rainfall interval. FER reflects the speed at which the flood spreads spatially, an important factor to consider in flood assessments, particularly in flash flood evaluations.

Generally, in flood hazard assessments the flood speed is not included. Flood interventions, especially Nature-based Solutions (NbS) focus on slowing down the surface runoff (Esraz-Ul-Zannat, Dedekorkut-Howes and Morgan, 2024). Responding to flash floods requires not only proper preparedness before the event but also a rapid response during the flood incidents (Archer and Fowler, 2018). Time is a critical factor in managing flash floods, especially when human resources are limited. Therefore, it is essential to have a measurable tool to assess flood agility and the effectiveness of flood prevention measures. In this context, FER fulfils this requirement. In addition, while FER assesses the speed of flood spreading, the Lag Interval (LI) plays a crucial role in mitigating the flood's impact. As shown in the experiments, the longer the lag time (LI), the lower the FER. In other words, a longer lag time helps reducing

661 the speed at which the flood expands in urban areas. By extending the LI, residents and
662 organizations in flood-prone regions would gain valuable time for preparation and evacuation.
663 Therefore, this temporal buffer is key to enhancing community resilience against flooding
664 events. Lengthening the LI could be an important strategy for mitigating flood impacts. It is
665 recommended to assess the influence of LI on flood reactions in urban areas to design more
666 effective flood interventions and reduce overall flood impact.

667 **Spatiotemporal Analysis**

668 Beside the temporal analysis, the spatiotemporal analysis provided a new perspectivee on the
669 spatial distribution of floods, integrating temporal dynamics into the assessment framework.
670 By accounting for flood sequences, the analytical approach followed here enabled to identify
671 areas prone to flooding over time, thus reshaped the priorities in flood management particularly
672 in the context of the rapid onset of extreme events. The selection and design of flood
673 interventions needs to take into account the temporary exposure of both the citizens (e.g. traffic
674 travellers) as well as the permanent residents in flood-prone areas. Spatiotemporal flood
675 evolution gives a holistic overview of the flood progress in both space and time during the
676 flooding time. This insight is vital to allocate human resources efficiently. In particular, this
677 information is very important both for stakeholders and citizens who live in a flood-prone area
678 for the development of an evacuation plan (Lee *et al.*, 2020). It will enable stakeholders such
679 as a drainage system company to allocate human resources during the rainfall event in order to
680 improve the effectiveness of maintenance plans.

681 **Spatiotemporal flood distribution pattern analysis**

682 Spatiotemporal flood distribution pattern analysis, compared to the use of solemnly static
683 topographic maps, reveals that initial flood-affected locations may not necessarily coincide

with areas of lowest elevation. Drainage efficiency decreases the flood risk of an area. This observation underscores the influence of the drainage system capacity on the flooding dynamics. It also reveals that high-intensity rainfall over a short period, or torrential rain, caused flooding in more concentrated areas. This highlights the sensitive regions vulnerable to flash floods in urban areas.

In addition, flood mitigation remedies must consider the cost-benefit balance. The size and location of interventions (i.e. swales, detention, retention) involve a spatial trade-off in urban planning design (Bush and Doyon, 2019). By incorporating a time scale, the spatiotemporal flood distribution increases the efficiency of the potential flood interventions.

This study showed that flooding caused by the historical rainstorm (pattern C) did not result in a high flood risk in low-intensity scenarios (i.e., 1.25-year, 2-year, 2.5-year, 5-year, and 10-year returned periods). The rainfall distribution interval (1 hour) appears to be the main factor behind this phenomenon. While pattern C has a 1-hour interval between rainfall events, patterns A and B have a 1-minute interval.

Limitations

Nevertheless, this study still has revealed some limitations. Firstly, this research relied on daily rainfall data for generating extreme rainfall events in the Monte Carlo simulations. While this ensures statistical reliability over a long period, it may smooth out short-duration, high-intensity peaks typically observed during monsoon events. As a result, the fixed hyetograph shape, while useful for general event simulation, might underestimate sub-daily peak intensities. This should be considered when interpreting the results, particularly for applications like urban flood modelling, where short-duration rainfall extremes can have significant impacts. Secondly, spatiotemporal flood distribution used IDW interpolation method which only based on the distance relation between the 1D spatiotemporal flood results.

This method has not yet taken into account the influence of DEM into the flood propagation. It is a trade-off between the speed and the accuracy of the modelling process. It is recommended to further research on 2D model which includes the DEM influence to the flood simulation. Furthermore, it is crucial to acknowledge that this study doesn't cover the entire spectrum of flood risk management. Factors such as socio-economic vulnerability and infrastructural resilience, which are equally vital components, should also be included to ensure a comprehensive flood risk assessment.

Future works

Although this work introduces a new approach for analysing floods that reshapes flood assessments, there is still room for further exploration. Firstly, the 2 new indicators (i.e. FER, LI) require further study to better understand their influence on urban flood response. Engaging these two indicators into the design of Nature-based solutions could boost the efficiency of these measurements. Secondly, applying the spatiotemporal analysis into a 2D model could enhance the quality of flood prediction. However, there may be a trade-off between modelling speed and accuracy when comparing the spatiotemporal 1D model and the spatiotemporal 2D model that needs to be considered. Monitoring urban flood data (e.g., floodwater quantity and quality) remains challenging due to limited human resources and the unpredictable distribution of rainfall. Therefore, the application of new technologies, such as machine learning and AI, could help reduce both the time and cost associated with flood research. Engaging citizens in data collection through crowdsourcing offers a potential solution to human resource shortages. This win-win approach benefits both citizens and researchers, providing a promising opportunity for effective data monitoring.

CONCLUSION

This study used an innovative methodological approach to delineate and analyse urban flood events by analyzing the direct correlation between rainfall patterns and the rate of drainage system saturation. By employing simplified models, we have captured the intricate spatial and temporal dynamics of urban flooding, underscoring the need to incorporate temporal sequencing and the timing of flood occurrences into comprehensive flood risk management.

This study has employed temporal analysis as a key component of flood response strategies. Through temporal and spatiotemporal assessments, we have highlighted the importance of prompt intervention in urban areas prone to flooding. The resulting temporal evolution diagrams and spatiotemporal flood distribution maps serve as essential tools, providing stakeholders with actionable insights and illustrating variations in flood expansion speeds across different scenarios. The introduction of the Flood Expansion Rate FER as a measurable indicator further refined our ability to evaluate and respond to flood risks with greater agility. The research proved that the spatiotemporal flood evolution pattern remains largely stable across different scenarios, confirming the reliability and importance of spatiotemporal analysis in the risk assessment process. Besides, the empirical findings revealed that the flooding patterns in the study area were not solely dictated by terrain elevations, indicating the presence of other significant factors influencing on flood behaviour. It is particularly noteworthy that the northern part of the drainage system shows a high level of flood prevention efficiency, attributed to its robust design conditions. While an analysis of the direct impact of specific flood events was beyond the scope of this study, the insights gained providing a clear indication of areas in need of enhanced drainage solutions and pinpointed locations with a recurring incidence of flooding. These findings are crucial for directing targeted infrastructure improvements and informing flood mitigation strategies.

Overall, the research contributed to a deeper understanding of flood dynamics and offers a foundation for future studies to build upon, particularly those aimed at quantifying the impacts of flooding events and refining urban flood management practices.

ACKNOWLEDGEMENTS

The authors would like to thank to Ministry of Infrastructure and Water Management – The Netherlands, IHE Delft Institute for Water Education – The Netherlands, The Viet Nam Government, Hanoi Drainage and Sewage System Company (HSDC) - Viet Nam, Hanoi Architectural University – Viet Nam, Ha Dong District People committee – Viet Nam, Yen Nghia Commune People Committee – Viet Nam and Yen Nghia citizens for supporting this research. This statement contained within the manuscript/research article are not opinions of the funding agency, Viet Nam Government or Dutch Government, but reflect the author's opinions.

The authors extend their gratitude to the reviewers for their insightful comments and valuable contributions to improving this manuscript.

FUNDING

This study is supported by Project 911 of Ministry of Education and Training - Viet Nam and Ministry of Infrastructure and Water Management - The Netherlands.

AUTHOR CONTRIBUTIONS

Conceptualization, H.D.M. and G.A.C.P.; methodology, H.D.M. and G.A.C.P.; software, H.D.M. and W.B.; formal analysis, H.D.M. and G.A.C.P.; investigation, H.D.M., G.A.C.P. and

W.B.; data curating, H.D.M.; writing – original draft preparation, H.D.M; writing – review and editing, H.D.M., G.A.C.P., W.B. and C.Z.; funding acquisition, H.D.M. and G.A.C.P.

CONFLICT OF INTEREST

The authors declare no conflict of interest.

None of authors affiliated or involved with any organization or was entity with any financial interest or non-financial interest in the subject matter and materials discussed in this paper.

DATA AVAILABILITY STATEMENT

Data supporting this study cannot be made available publicly due to privacy of stakeholders; reader should contact the corresponding author for details.

REFERENCES

Abedin, J. *et al.* (2024) "Deciphering spatial-temporal dynamics of flood exposure in the United States," *Sustainable Cities and Society*, 108(October 2023), p. 105444. Available at: https://doi.org/10.1016/j.scs.2024.105444.

Acosta-Coll, M. *et al.* (2018) "Real-time early warning system design for pluvial flash floods—a review," *Sensors (Switzerland)*, 18(7). Available at: https://doi.org/10.3390/s18072255.

Afsari, R. *et al.* (2022) "A Spatial Decision Support Approach for Flood Vulnerability Analysis in Urban Areas: A Case Study of Tehran," *ISPRS International Journal of Geo-Information*, 11(7), p. 380. Available at: https://doi.org/10.3390/ijgi11070380.

Archer, D.R. and Fowler, H.J. (2018) "Characterising flash flood response to intense rainfall and impacts using historical information and gauged data in Britain," *Journal of Flood Risk Management*, 11, pp. S121–S133. Available at: https://doi.org/10.1111/jfr3.12187.

795 Arrighi, C., Oumeraci, H. and Castelli, F. (2017) “Hydrodynamics of pedestrians’ instability
796 in floodwaters,” *Hydrology and Earth System Sciences*, 21(1), pp. 515–531. Available at:
797 https://doi.org/10.5194/hess-21-515-2017.
798 Beg, M.N.A. *et al.* (2020) “CFD modelling of the transport of soluble pollutants from sewer
799 networks to surface flows during urban flood events,” *Water (Switzerland)*, 12(9). Available
800 at: https://doi.org/10.3390/w12092514.
801 Bentivoglio, R. *et al.* (2023) “Rapid spatio-Temporal flood modelling via hydraulics-based
802 graph neural networks,” *Hydrology and Earth System Sciences*, 27(23), pp. 4227–4246.
803 Available at: https://doi.org/10.5194/hess-27-4227-2023.
804 Berkhahn, S. and Neuweiler, I. (2024) “Data driven real-time prediction of urban floods with
805 spatial and temporal distribution,” *Journal of Hydrology X*, 22(October 2023), p. 100167.
806 Available at: https://doi.org/10.1016/j.hydroa.2023.100167.
807 Bernardini, G. *et al.* (2024) “Assessing the spatiotemporal impact of users’ exposure and
808 vulnerability to flood risk in urban built environments,” *Sustainable Cities and Society*,
809 100(September 2023). Available at: https://doi.org/10.1016/j.scs.2023.105043.
810 Burrichter, B. *et al.* (2023) “A Spatiotemporal Deep Learning Approach for Urban Pluvial
811 Flood Forecasting with Multi-Source Data,” *Water (Switzerland)*, 15(9). Available at:
812 https://doi.org/10.3390/w15091760.
813 Bush, J. and Doyon, A. (2019) “Building urban resilience with nature-based solutions: How
814 can urban planning contribute?,” *Cities*, 95(July), p. 102483. Available at:
815 https://doi.org/10.1016/j.cities.2019.102483.
816 Chang, L.C., Liou, J.Y. and Chang, F.J. (2022) “Spatial-temporal flood inundation nowcasts
817 by fusing machine learning methods and principal component analysis,” *Journal of Hydrology*,
818 612(PA), p. 128086. Available at: https://doi.org/10.1016/j.jhydrol.2022.128086.

819 Corzo Perez, G.A. *et al.* (2024) “Development of a hazard risk map for assessing pedestrian
820 risk in urban flash floods: A case study in Cúcuta, Colombia,” *River*, 3(1), pp. 8–23. Available
821 at: https://doi.org/10.1002/rvr2.78.
822 Darnkachatarn, S. and Kajitani, Y. (2024) “Long-term flood exposure assessment using
823 satellite-based land use change detection and inundation simulation: A 30-year case study of
824 the Bangkok Metropolitan Region,” *Journal of Flood Risk Management*, 17(3), pp. 1–16.
825 Available at: https://doi.org/10.1111/jfr3.12997.
826 Dong, B. *et al.* (2022) “Risk assessment for people and vehicles in an extreme urban flood:
827 Case study of the ‘7.20’ flood event in Zhengzhou, China,” *International Journal of Disaster*
828 *Risk Reduction*, 80(August). Available at: https://doi.org/10.1016/j.ijdrr.2022.103205.
829 England, J.F. *et al.* (2019) *Guidelines for determining flood flow frequency-Bulletin 17C*,
830 *Techniques and Methods, book 4, chap. B5*.
831 Esraz-Ul-Zannat, M., Dedekorkut-Howes, A. and Morgan, E.A. (2024) “A review of nature-
832 based infrastructures and their effectiveness for urban flood risk mitigation,” *Wiley*
833 *Interdisciplinary Reviews: Climate Change*, (April), pp. 1–28. Available at:
834 https://doi.org/10.1002/wcc.889.
835 Fang, B. *et al.* (2024) “An increase in the spatial extent of European floods over the last 70
836 years,” *Hydrology and Earth System Sciences*, 28(16), pp. 3755–3775. Available at:
837 https://doi.org/10.5194/hess-28-3755-2024.
838 Fernández-Nóvoa, D., González-Cao, J. and García-Feal, O. (2024) “Enhancing Flood Risk
839 Management: A Comprehensive Review on Flood Early Warning Systems with Emphasis on
840 Numerical Modeling,” *Water (Switzerland)*, 16(10). Available at:
841 https://doi.org/10.3390/w16101408.

842 Francipane, A. *et al.* (2021) “A paradigm of extreme rainfall pluvial floods in complex urban
843 areas: The flood event of 15 July 2020 in Palermo (Italy),” *Natural Hazards and Earth System*
844 *Sciences*, 21(8), pp. 2563–2580. Available at: https://doi.org/10.5194/nhess-21-2563-2021.
845 Getirana, A. *et al.* (2023) “An urban drainage scheme for large-scale flood models,” *Journal*
846 *of Hydrology*, 627(PA), p. 130410. Available at:
847 https://doi.org/10.1016/j.jhydrol.2023.130410.
848 Güneralp, B., Güneralp, I. and Liu, Y. (2015) “Changing global patterns of urban exposure to
849 flood and drought hazards,” *Global Environmental Change*, 31, pp. 217–225. Available at:
850 https://doi.org/10.1016/j.gloenvcha.2015.01.002.
851 Hauser, M. *et al.* (2024) “The Impact of Underground Structures on Urban Flood Models,”
852 *Water (Switzerland)*, 16(1), pp. 1–12. Available at: https://doi.org/10.3390/w16010170.
853 Henonin, J. *et al.* (2013) “Real-time urban flood forecasting and modelling - A state of the art,”
854 *Journal of Hydroinformatics*, 15(3), pp. 717–736. Available at:
855 https://doi.org/10.2166/hydro.2013.132.
856 Ho, T.M.H. *et al.* (2011) “Extreme climatic events over Vietnam from observational data and
857 RegCM3 projections,” *Climate Research*, 49(2), pp. 87–100. Available at:
858 https://doi.org/10.3354/cr01021.
859 Huynh, T.T.N. *et al.* (2019) “Enteric pathogens in flood-related waters in urban areas of the
860 Vietnamese Mekong Delta: a case study of Ninh Kieu district, Can Tho city,” *Urban Water*
861 *Journal*, 16(9), pp. 634–641. Available at: https://doi.org/10.1080/1573062X.2020.1713381.
862 Kuller, M., Schoenholzer, K. and Lienert, J. (2021) “Creating effective flood warnings: A
863 framework from a critical review,” *Journal of Hydrology*, 602(June), p. 126708. Available at:
864 https://doi.org/10.1016/j.jhydrol.2021.126708.
865 Kundzewicz, Z.W. and Pińskwar, I. (2022) “Are Pluvial and Fluvial Floods on the Rise?,”
866 *Water (Switzerland)*, 14(17), pp. 1–16. Available at: https://doi.org/10.3390/w14172612.

867 Lameche, E. khansa *et al.* (2023) "Urban flood numerical modeling and hydraulic performance
868 of a drainage network: A case study in Algiers, Algeria," *Water Science and Technology*, 88(7),
869 pp. 1635–1656. Available at: https://doi.org/10.2166/wst.2023.277.
870 Leandro, J. *et al.* (2009) "Comparison of 1D/1D and 1D/2D Coupled (Sewer/Surface)
871 Hydraulic Models for Urban Flood Simulation," *Journal of Hydraulic Engineering*, 135(6), pp.
872 495–504. Available at: https://doi.org/10.1061/(ASCE)HY.1943-7900.0000037.
873 Leandro, J., Schumann, A. and Pfister, A. (2016) "A step towards considering the spatial
874 heterogeneity of urban key features in urban hydrology flood modelling," *Journal of*
875 *Hydrology*, 535, pp. 356–365. Available at: https://doi.org/10.1016/j.jhydrol.2016.01.060.
876 Lee, Y.H. *et al.* (2020) "Flood evacuation routes based on spatiotemporal inundation risk
877 assessment," *Water (Switzerland)*, 12(8). Available at: https://doi.org/10.3390/w12082271.
878 Levin, N. and Phinn, S. (2022) "Assessing the 2022 Flood Impacts in Queensland Combining
879 Daytime and Nighttime Optical and Imaging Radar Data," *Remote Sensing*, 14(19). Available
880 at: https://doi.org/10.3390/rs14195009.
881 Li, Q. *et al.* (2023) "Risk assessment of individuals exposed to urban floods," *International*
882 *Journal of Disaster Risk Reduction*, 88(February), p. 103599. Available at:
883 https://doi.org/10.1016/j.ijdrr.2023.103599.
884 Liu, T., Shi, P. and Fang, J. (2022) "Spatiotemporal variation in global floods with different
885 affected areas and the contribution of influencing factors to flood-induced mortality (1985–
886 2019)," *Natural Hazards*, 111(3), pp. 2601–2625. Available at:
887 https://doi.org/10.1007/s11069-021-05150-5.
888 Luo, P. *et al.* (2018) "Flood inundation assessment for the Hanoi Central Area, Vietnam under
889 historical and extreme rainfall conditions," *Scientific Reports*, 8(1), pp. 1–11. Available at:
890 https://doi.org/10.1038/s41598-018-30024-5.

Mahiddin, N.A., Umar, R. and Rajan, N. (2023) “Rising Water, Rising Voices: Empowering Communities Through The Flood Emergency Response Plan,” *E3S Web of Conferences*, 437, pp. 1–9. Available at: https://doi.org/10.1051/e3sconf/202343702009.

Do Minh, H. *et al.* (2023) “A Spatiotemporal hydrological response of extreme urban floods in Ha Noi – Vietnam,” in. Vienna, Austria: EGU General Assembly 2023, Vienna, Austria, 24-28 Apr 2023, EGU23 - 6891. Available at: https://doi.org/https://doi.org/10.5194/egusphere-egu23-6891, 2023.

Ministry of Construction of Viet Nam (2006) *Water Supply - Distribution System and Facilities Design Standard*, *Construction Publisher - Nhà xuất bản xây dựng*. Vietnam.

Mishra, S.P., Sethi, K.C. and Siddique, M. (2020) “Emerging threats during anthropocene as urban flooding of bhubaneswar city, India,” *Water and Energy International*, 63r(1), pp. 46–58.

Nguyen, H.Q. *et al.* (2017) “Water Quality Dynamics of Urban Water Bodies during Flooding in Can Tho City, Vietnam,” *Water*, 9(4), p. 260. Available at: https://doi.org/10.3390/w9040260.

Olsson, G. (2019) “Controlling Urban Drainage Systems,” in *New Trends in Urban Drainage Modelling*. Springer International Publishing, pp. 191–206. Available at: https://doi.org/10.1007/978-3-319-99867-1_33.

Pham Thi, H. *et al.* (2019) “Determination of the relationship between Vietnam national coordinate reference system (VN-2000) and ITRS, WGS84 and PZ-90,” *E3S Web of Conferences*, 94. Available at: https://doi.org/10.1051/e3sconf/20199403014.

Piadeh, F., Behzadian, K. and Alani, A.M. (2022) “A critical review of real-time modelling of flood forecasting in urban drainage systems,” *Journal of Hydrology*, 607(January), p. 127476. Available at: https://doi.org/10.1016/j.jhydrol.2022.127476.

915 Pichler, M. (2022) “swmm_api: API for reading, manipulating and running SWMM-Projects
916 with python (0.3).” Zenodo. Available at:
917 https://doi.org/https://doi.org/10.5281/zenodo.7054804.
918 Prokić, M., Savić, S. and Pavić, D. (2019) “Pluvial flooding in Urban Areas Across the
919 European Continent,” *Geographica Pannonica*, 23(4), pp. 216–232. Available at:
920 https://doi.org/10.5937/gp23-23508.
921 Qin, J. *et al.* (2024) “A novel and efficient method for real-time simulating spatial and temporal
922 evolution of coastal urban pluvial flood without drainage network,” *Environmental Modelling
923 and Software*, 172(November 2023), p. 105888. Available at:
924 https://doi.org/10.1016/j.envsoft.2023.105888.
925 Sañudo, E. *et al.* (2024) “Large-scale physical facility and experimental dataset for the
926 validation of urban drainage models,” *Hydrological Processes*, 38(1), pp. 1–14. Available at:
927 https://doi.org/10.1002/hyp.15068.
928 Schanze, J. (2018) “Pluvial flood risk management: an evolving and specific field,” *Journal of
929 Flood Risk Management*, 11(3), pp. 227–229. Available at: https://doi.org/10.1111/jfr3.12487.
930 Schmid, F. and Leandro, J. (2024) “A Data-Driven Multi-Step Flood Inundation Forecast
931 System,” *Forecasting*, 6(3), pp. 761–781. Available at:
932 https://doi.org/10.3390/forecast6030039.
933 Seyoum, S.D. *et al.* (2012) “Coupled 1D and Noninertia 2D Flood Inundation Model for
934 Simulation of Urban Flooding,” *JOURNAL OF HYDRAULIC ENGINEERING © ASCE*,
935 138(1), pp. 23–34. Available at: https://doi.org/10.1061/(ASCE)HY.1943-7900 .0000485.
936 Shin, E. *et al.* (2021) “Spatiotemporal flood risk assessment of underground space considering
937 flood intensity and escape route,” *Natural Hazards*, 109(2), pp. 1539–1555. Available at:
938 https://doi.org/10.1007/s11069-021-04888-2.

939 Tanaka, T., Kiyohara, K. and Tachikawa, Y. (2020) “Comparison of fluvial and pluvial flood
940 risk curves in urban cities derived from a large ensemble climate simulation dataset: A case
941 study in Nagoya, Japan,” *Journal of Hydrology*, 584(September 2019), p. 124706. Available
942 at: https://doi.org/10.1016/j.jhydrol.2020.124706.
943 U.S. Advisory committee on water data (1982) “Guidelines for determining flood flow
944 frequency.”
945 Vasconcelos, J.G. *et al.* (2024) “Evolution and Characterization of Pressurized Flow
946 Conditions in Stormwater Collection Networks,” *Journal of Hydraulic Engineering*, 150(2).
947 Available at: https://doi.org/10.1061/jhend8.hyeng-13835.
948 Vietnam Government (2006) *Nghị định về việc thành lập thành phố Hà Đông thuộc tỉnh Hà*
949 *Tây -Decree of establishing Ha Dong city, Ha Tay province*, *Vietnam Government*. Vietnam.
950 Vietnam Government (2008) *Nghị định về việc điều chỉnh địa giới hành chính xã, phường, để*
951 *thành lập phường thuộc thành phố Hà Đông, thành phố Sơn Tây, tỉnh Hà Tây - Decree of*
952 *adjusting administrative boundaries of communes, wards to establish wards in Ha Dong city*
953 *and Son Tay city*. Viet Nam.
954 Wang, L. *et al.* (2022) “A review of the flood management: from flood control to flood
955 resilience,” *Heliyon*, 8(11), p. e11763. Available at:
956 https://doi.org/10.1016/j.heliyon.2022.e11763.
957 Wijaya, O.T. *et al.* (2023) “A rapid flood inundation model for urban flood analyses,”
958 *MethodsX*, 10(April), p. 102202. Available at: https://doi.org/10.1016/j.mex.2023.102202.
959 Yen Nghia Comune People’s comittee (2019) *The 2019 Viet Nam population and housing*
960 *cencus*.
961 Zhou, R. *et al.* (2022) “Flood impacts on urban road connectivity in southern China,” *Scientific*
962 *Reports*, 12(1), pp. 1–17. Available at: https://doi.org/10.1038/s41598-022-20882-5.

963 Zhou, Y. *et al.* (2025) “Incorporating hydrological constraints with deep learning for
964 streamflow prediction,” *Expert Systems with Applications*, 259(September 2024), p. 125379.
965 Available at: https://doi.org/10.1016/j.eswa.2024.125379.
966 Zhou, Z. *et al.* (2021) “The impact of the spatiotemporal structure of rainfall on flood frequency
967 over a small urban watershed: An approach coupling stochastic storm transposition and
968 hydrologic modeling,” *Hydrology and Earth System Sciences*, 25(9), pp. 4701–4717. Available
969 at: https://doi.org/10.5194/hess-25-4701-2021.
970 Zhu, Z. *et al.* (2023) “Effect of urban neighbourhood layout on the flood intrusion rate of
971 residential buildings and associated risk for pedestrians,” *Sustainable Cities and Society*,
972 92(October 2022), p. 104485. Available at: https://doi.org/10.1016/j.scs.2023.104485.
973